Energy Geoscience 3 (2022) 235–254

Contents lists available at ScienceDirect

Energy Geoscience

journal homepage: www.keaipublishing.com/en/journals/energy-geoscience

Bowland Shale well placement strategy – Part 2: Fracture simulations using a 3D geomechanical model and implications for stratigraphic and spatial horizontal well locations

Iain de Jonge-Anderson [a, *], Jingsheng Ma [a], Xiaoyang Wu [b], Dorrik Stow [a], David Griffiths [c]

[a] Institute of GeoEnergy Engineering (IGE), School of Energy, Geoscience, Infrastructure & Society, Heriot-Watt University, Edinburgh, EH14 4AS, UK
[b] British Geological Survey, The Lyell Centre, Research Avenue South, Edinburgh, EH14 4AP, UK
[c] Penrhyn Exploration, UK

ARTICLE INFO

Article history:
Received 17 September 2021
Received in revised form
3 March 2022
Accepted 23 March 2022

Keywords:
Bowland Shale
Hydraulic fracturing
Geomechanics
Fracture simulation
Well placement

ABSTRACT

Hydraulic fracture modelling is a key component of a shale reservoir well placement strategy as it provides an indication of the typical lengths and heights of stimulated fractures and of the changes to the stress environment in which these are propagating. However, spatial and stratigraphic variations in the stress and geomechanical properties of shales make accurate modelling a challenging task. For the UK Bowland Shale, stacked horizontal wells targeting multiple stratigraphic intervals could be used to avoid large offset faults in a geologically complex area. However, it is not known how these intervals may respond to hydraulic fracturing and predicting the height and length of hydraulic fractures is necessary in order to assess the likelihood of vertical fracture interference across landing zones or propagation towards major faults. In the case of the former, intervals of high effective stress may be key to containing fractures within their desired target. Using a planar hydraulic fracture simulator, and a 3D geomechanical model incorporating dipping stratigraphy, the issue of predicting hydraulic fracture geometry in the Bowland Shale was assessed through a series of modelling exercises using well Preese Hall-1 and horizontal pseudo-wells. When pre-defined landing zones were targeted, narrow and long transverse fractures around 1 km from the well were simulated. When the simulation design mimicked perforation clusters placed at 12 m intervals along horizontal pseudo-wells, the effects of stress shadowing were acute and resulted in irregular fracture geometries. Furthermore, high effective stress intervals performed efficiently as barriers to vertical hydraulic fracture propagation, reinforcing the feasibility of using stacked production for the Bowland Shale. The modelling results were then used to discuss the possible placement of horizontal wells in a mapped, 100 km^2 region around well Preese Hall-1, where up to 13 sites could be positioned, with a horizontal well length of around 1.5 km. Finally, by drawing on a well-established analogue for the Bowland Shale, it was estimated that up to 195 Bcf of gas could be produced from the 13 locations in the area if three stratigraphic intervals are produced from one location.

1. Introduction

The use of hydraulic fracturing to exploit unconventional resources from tight shales or others, has transformed the global energy industry in the early 21st Century. Whilst the technology has been deployed most successfully in the USA, several other countries have also sought to enhance their domestic hydrocarbon production similarly, including China, Canada and Argentina. In the UK, the Mississippian Bowland Shale Formation of north England is the most prospective shale gas target (Smith et al., 2010), though estimates of the precise size of the resource vary considerably (Andrews, 2013; Whitelaw et al., 2019). In the Craven Basin, where exploration has focused thus far, the formation displays good reservoir properties (Clarke et al., 2014a, 2018; de Jonge-Anderson et al., 2021a) ; however, it also exhibits acute sedimentological

* Corresponding author.
E-mail address: i.anderson@hw.ac.uk (I. de Jonge-Anderson).

Production and Hosting by Elsevier on behalf of KeAi

https://doi.org/10.1016/j.engeos.2022.03.004

(Emmings et al., 2020) and microtextural (Fauchille et al., 2017) heterogeneity and is located within a complex structural setting (de Jonge-Anderson and Underhill, 2020). A full test of the producibility of the formation is yet to be conducted, with early attempts being suspended prematurely due to elevated levels of induced seismicity (Clarke et al., 2014b, 2019b; Verdon et al., 2019, 2020). The structural complexity and the levels of induced seismicity observed during hydraulic fracturing, have led to some questions if drilling long horizontal wells is an appropriate strategy for the Bowland Shale (de Jonge-Anderson and Underhill, 2020).

This paper is the second of a two-part series that proposes an alternative well placement strategy for the Bowland Shale, specifically assessing the constraints of faulting and heterogeneous rock properties on hydraulic fracture propagation. In Part 1 (de Jonge-Anderson et al., 2021b), a series of wireline log-derived models were used to form a classification of the geomechanical units within the Bowland Shale at well Preese Hall-1 (PH-1), drilled in the Craven Basin (Fig. 1) in 2010. A cluster model was used to identify the intervals that held the best geomechanical properties, of which three were proposed as good candidates for landing horizontal wells.

The second paper continues with a modelling study of the fracture characteristics of the Bowland Shale. A series of fracture simulations were designed, both along the vertical well PH-1 itself and along horizontal pseudo-wells targeting the three landing zones. The simulations were designed to answer a series of important questions about the well placement strategy for producing gas from the shale. Firstly, what geometries could be expected from hydraulic fractures generated in the shale? Secondly, are fracture barriers (zones of high effective stress) present within the stratigraphic section? Thirdly, what length of horizontal well could be drilled and stimulated without the modelled hydraulic fractures and the wellbore itself encountering seismic-scale faults and finally, what are the consequences of these observations for the extractable resources?

2. Background

2.1. Constraints imposed by geological structure

Mapping of the Carboniferous sequences around well PH-1 (including the Lower Bowland Shale) was undertaken by de Jonge-Anderson and Underhill (2020) using a 3D seismic dataset. The quality of this dataset was variable, and while it allowed for the main, large-offset faults to be recognised, these were often mapped using an absence of clear seismic reflectivity rather than offset of

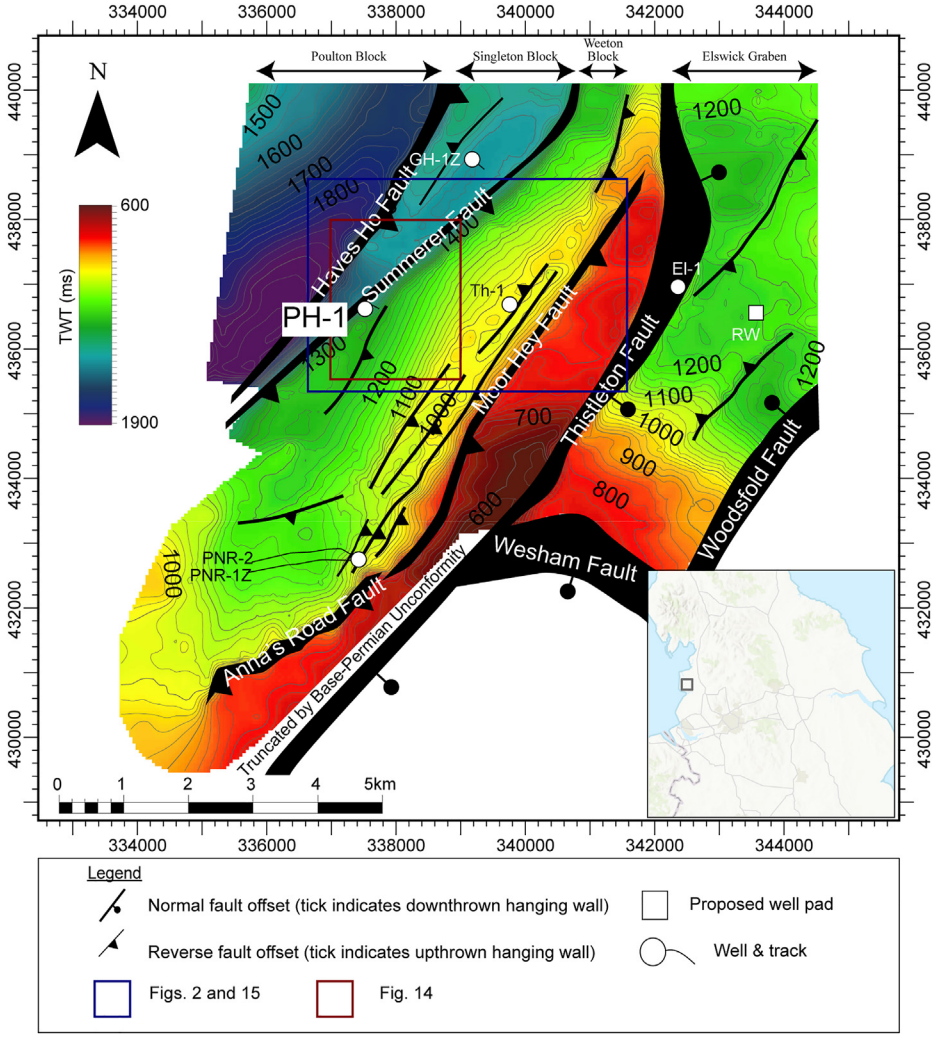

Fig. 1. Two-way time-structure map for the Lower Bowland Shale in an area of the Craven Basin highlighting well PH-1, additional wells and interpreted faults (after de Jonge-Anderson and Underhill, 2020). Also shown are the locations of Figs. 2, 14 and 15. Note: El-1. Elswick-1; GH-1Z. Grange Hill-1Z; Th-1. Thistleton-1; PNR. Preston New Road-1; RW. Roseacre Wood.

the seismic reflectors (de Jonge-Anderson and Underhill, 2020), resulting in some uncertainty regarding their precise position. The study concluded that the area around well PH-1 is characterised by steep reverse faults and folded strata that in turn, compartmentalise and deform the Bowland Shale (Fig. 1) (de Jonge-Anderson and Underhill, 2020). As a consequence, if horizontal wells are to be drilled along the direction of minimum horizontal stress, the maximum length that may be achieved within each fault block is typically less than 2 km (de Jonge-Anderson and Underhill, 2020).

However, a further challenge is posed by the geometrical mismatch between the orientation of major faults and the maximum horizontal stress orientation, along which hydraulic fractures will be likely to propagate. The minimum horizontal stress is oriented along an azimuth of ~080° (Clarke et al., 2014a), which is represented as a black line extending from well PH-1, east, towards the Moor Hey Fault in Fig. 2. The well was drilled on the western edge of the Weeton Block, bound by the Summerer Fault to the north-west and the Moor Hey Fault to the south-east (Fig. 1). The width of this block along the minimum horizontal stress orientation is ~3 km, and if a lateral section was side-tracked from well PH-1 along this azimuth, a length of ~2.5 km could be achieved before the Moor Hey Fault was encountered.

However, as the maximum horizontal stress orientation and the strike of the major faults are not parallel as estimated (de Jonge-Anderson and Underhill, 2020), there is a risk of hydraulic fractures interacting with these faults at the heel and toe of such a hypothetical well. Near the heel, there is a risk of hydraulic fractures propagating north and interacting with the Summerer Fault, whereas near the toe of the well, there is a risk of hydraulic fractures propagating south and interacting with the Moor Hey Fault (Fig. 2). Assessing the risks and emplacing completion stages accordingly will require knowledge of the expected fracture propagation lengths. Naturally, the risk of causing induced seismicity depends on whether the associated faults are critically stressed. However, even if this were not the case, hydraulic fractures interfering with such structures may still ultimately deflect the imposed energy from fracturing the desired matrix around the wellbore and would be detrimental to production.

2.2. Well PNR-1Z

While this work focuses on well PH-1, treatment data relating to the hydraulic fracturing of an adjacent well, well PNR-1Z, was used to design a typical horizontal well for simulation. well PNR-1Z is a horizontal well side-tracked from the semi-vertical well PNR-1, both drilled by Cuadrilla Resources over a period between September 2017 and April 2018. The site is located ~4 km south of well PH-1 (Fig. 1) but also within the Weeton fault block (de Jonge-Anderson and Underhill, 2020). It comprises a 782 m horizontal section targeting the Lower Bowland Shale that was subsequently stimulated between October and December 2018. High levels of induced seismicity were encountered during hydraulic fracturing operations, resulting in only part of the full treatment schedule completed (Clarke et al., 2019b).

Because of the induced seismicity at well PNR-1Z, a comprehensive dataset relating to the hydraulic fracturing operations was made publicly available by the North Sea Transition Authority (North Sea Transition Authority, 2019). The dataset consists of daily operation reports, fracture sleeve depths, fluid and proppant pumping schedules and recorded microseismic activities. For this work, data relating to the well trajectory, completion setup and pumping schedules from well PNR-1Z were used to design representative pseudo-wells at well PH-1 for simulation.

2.3. Fracture barriers

Stacked horizontal drilling may form a viable production strategy for the Bowland Shale (Clarke et al., 2014a, 2018), and analysis presented in Part 1 of this series (de Jonge-Anderson et al., 2021b) concluded that multiple intervals exist within the stratigraphic section in Well PH-1 that exhibit excellent geomechanical properties (low effective stress, low fracture toughness and high

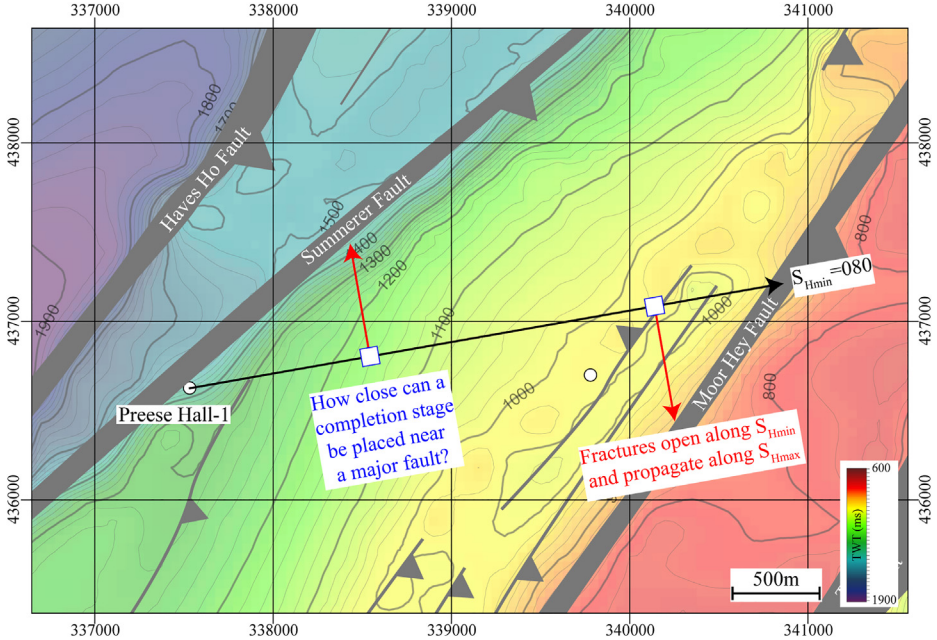

Fig. 2. Lower Bowland Shale time structure map near well PH-1 (after de Jonge-Anderson and Underhill, 2020), the location of which is shown in Fig. 1. A hypothetical lateral well is drawn from well PH-1, along the azimuth of minimum horizontal stress up to the Moor Hey Fault. The image exemplifies the geometrical problem posed by mapped faults whose strike is not parallel to maximum horizontal stress orientation. If a well is drilled near the edge of a fault block (as the case at well PH-1), there is a risk of hydraulic fractures interfering with those block-defining faults.

brittleness). However, barriers to fracture propagation including high effective-stress intervals (Simonson et al., 1978; Jeffrey and Bunger, 2009) and rock property contrasts (Xu et al., 2019) are also key components of a successful shale play as these play a role in containing hydraulic fractures within the desired interval.

Tight limestones have proven successful fracture barriers in effective shale plays in the US, such as the Tully and Onandaga Limestones bounding the Marcellus Shale (Zhang, 2019) and the Viola/Simpson and Marble Falls Limestones bounding the Barnett Shale (Bowker, 2003; Pollastro et al., 2007). Similarly, the Wolfcamp Formation in the Permian Basin, which is targeted using stacked horizontal wells, contains several thinner limestones that form barriers to vertical hydraulic fracture growth (Parsegov et al., 2018; Rutledge et al., 2018; Stegent and Candler, 2018). But conversely, clay-rich intervals can also form efficient fracture barriers (Mullen, 2010). This suggests that identifying fracture barriers cannot be performed using lithology alone, and further analysis of stress and geomechanical properties is necessary.

In Part 1 of this series (de Jonge-Anderson et al., 2021b), geomechanical characteristics were used to highlight high effective-stress zones of the shale that may be suitable barriers to fracture growth. Whether these zones are of adequate thickness or magnitude to prevent well interference is a question further addressed in this paper.

2.4. Hydraulic fracture models

To model the propagation of transverse and longitudinal fractures within the Bowland Shale, a numerical 3D hydraulic fracture modelling software package, GOHFER (Grid Oriented Hydraulic Fracture Extension Replicator), was used. Fracture models such as GOHFER take physical laws relating to fluid, solid, fracture and thermal mechanics to simulate fracture geometry. These can be crudely classified into three categories with computational complexity increased: 2D models, pseudo-3D models, and planar-3D models. The background theory to such models can be found in the comprehensive reviews of Warpinski et al. (1993a) and Mack and Warpinski (2000). GOHFER is a planar-3D-type fracture model that was developed by Barree (1983a, 1983b) and its ability to handle a 3D input grid of geomechanical properties has made it a popular tool for predicting complex hydraulic fracture geometries.

2.5. Stress shadowing theory

The drive to increase the productivity of shale plays has resulted in operators drilling increasingly long horizontal wells with numerous perforation clusters along their lateral sections, ensuring maximum stimulation of the target reservoir. However, field observations including analysis of treatment pressure responses (Simpson et al., 2016; Skomorowski et al., 2015) and microseismic patterns (Fisher et al., 2004; Nagel and Sanchez-Nagel, 2011) suggest that hydraulic fractures alter the subsurface stress state to such a degree that subsequent fracturing stages can perform less efficiently. Numerical studies focusing on the changing stress state around a hydraulic fracture (Morrill and Miskimins, 2012; Nagel et al., 2013a, 2013b; Nagel and Sanchez-Nagel, 2011; Rios et al., 2013) suggest that the inter-fracture region experiences an increase in minimum horizontal stress, which then, in turn, makes that area more resistant to subsequent hydraulic fracturing. The increase in minimum horizontal stress owing to the stress shadow effect can be expressed as 'transmitted' stress from one fracture plane to another (Barree, 2015). In the GOHFER simulator, Boussinesq (1885)'s stress solution is used to consider the decay in stress with distance around a propagating fracture with the rate of decay controlled by the transverse exponent (t). The equation for transmitted stress (σ) then becomes (Barree, 2015):

$$\sigma = \frac{wE}{12Z^{t}} \tag{1}$$

Where w is the fracture width of adjacent planar fracture, E is the Young's modulus of the rock and Z is the distance from the adjacent planar fracture. The transverse exponent (t) typically ranges from 1.2 (plane strain case and strong fracture interference) to 2 (point load case and no fracture interference) (Barree, 2015).

3. Methodology

3.1. Input data

The primary input to GOHFER is the fracture closure stress (the stress that needs to be overcome to initiate the opening of a fracture) of the rock. Provided the tectonic setting is not one of compression, the fracture closure stress, minimum horizontal stress, and least principal stress are considered equivalent, which are often used interchangeably. The model is designed to handle well logs and implements the same equation for minimum horizontal stress as used in Part 1 of this series (de Jonge-Anderson et al., 2021b).

In addition to the fracture closure stress, the net pressure (also referred to as process-zone stress, PZS) is another important parameter to consider when determining the fracture characteristics of a material. It is equivalent to the net pressure above closure stress (Ramurthy and Hendrickson, 2007) required for the fracture to propagate (Belyadi et al., 2017). To estimate PZS, results from mini-frac analysis (De Pater and Pellicer, 2011; courtesy of Cuadrilla Resources) at well PH-1 were first added to the calibration dataset for stages 1–3, which is outlined in Table 1.

Following this, a continuous log of PZS was calculated using a linear transform of effective porosity, calibrated to the measured PZS value (Halliburton, 2019):

$$PZS = PZS_{\mathrm{Max}} + PHIE{*}k \tag{2}$$

Where:

$$k = -(PZS_{\mathrm{Contrast}}{*}PZS_{\mathrm{Max}})/PHIE_{\mathrm{Max}} \tag{3}$$

Referring to the PZS calibration points in Table 1, it was found that PZS_{Max} set to 8 MPa whilst keeping PZS_{Contrast} and $PHIE_{\mathrm{Max}}$ at their default values (1 and 0.25 respectively), could produce a reasonable fit to the data (Fig. 3).

3.2. Gridding and upscaling of log properties

GOHFER simulates a 3D planar fracture propagating within a 3D geological model. Such a geological model is referred to as a grid; a series of cells that contain upscaled stress and rock properties are derived from the input data.

3.2.1. Orientation and structure of the grid

The grid can be described as consisting of a longitudinal axis (*A-A'*; Fig. 4a and b) which is in parallel to the orientation of minimum horizontal stress, and a transverse axis (*B–B'*; Fig. 4a and c) which is parallel to the orientation of maximum horizontal stress. In subsequent sections, whilst describing the simulation setup, simulated fractures are described as either longitudinal or transverse, in alignment with these orientations, accordingly. The limits of the grid in the transverse direction were set to be 2000 m away from the well, and in the plots presented in later sections of the paper,

Table 1
Pore pressure, closure stress and process zone stress values from minifrac tests conducted across three stages of well PH-1 and collated from De Pater and Pellicer (2011) and Clarke et al. (2019a). The depths quoted are the arithmetic average taken over the complete stage interval which can be up to 70 m in size.

Stage	Depth (MD-M)	Pore Pressure (MPa)	Closure Stress (MPa)	Process Zone Stress (MPa)
3	2577	35.1	44.5	6.4
2	2661	37.9	49.8	7.7
1	2711	37.3	44.1	6.4

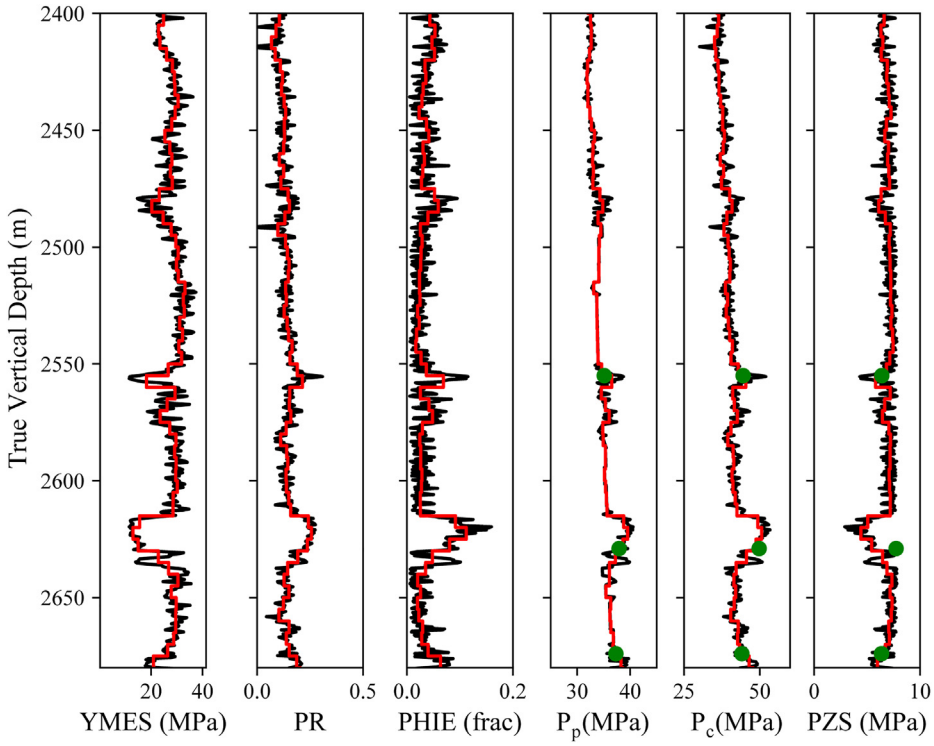

Fig. 3. Log display illustrating the input logs used for the hydraulic fracturing simulation. From left to right, YMES is Static Young's modulus, PR is Poisson's ratio, PHIE is effective porosity, P_p is pore pressure, Pc is closure pressure, and PZS is process zone stress. The black curves represent the wireline logs used as inputs to the simulations. The blocky red logs represent the equivalent logs, upscaled to 5 m vertical grid size and the green dots represent the calibration points shown in Table 1.

the x-axis refers to this distance, expressed either as positive (where the fracture propagates to the north) or negative (where the fracture propagates to the south) figures.

For all simulations, the grid size was set to be 5 m in the X, Y and Z directions. As a result, the wireline log-derived input data (black curves in Fig. 3) were upscaled to this resolution (red, blocky curves in Fig. 3) and extrapolated away from the well in 3D space. Whilst the simulations presented in Section 4 used a layer-cake geological grid consisting of flat-lying stratigraphy, the simulations presented in Section 5 used a tilted grid (Fig. 4b and c) to reflect the highly-dipping beds east of well PH-1 (de Jonge-Anderson and Underhill, 2020).

3.3. Pumping schedule

The increase in fluid pressure which drives the propagation of fractures within the hydraulic fracture software is achieved by simulating a hydraulic fracturing treatment at the appropriate completion interval. For this work, slickwater hydraulic fracturing treatments similar to that conducted at well PNR-1Z were simulated.

The key elements of a slickwater hydraulic fracturing job are the pumping rate of the fluid (water and chemicals) and the proppant concentration. A typical job will include a steady pump rate, but with the proppant concentration progressively increased ('ramped') either smoothly or in steps. At well PNR-1Z, where the first multi-stage slickwater hydraulic fracturing in the Bowland Shale was undertaken, the operations were designed such that 400 m^3 of fluid and 50 t of proppant were to be pumped into each stage (North Sea Transition Authority, 2019).

For this work, a single treatment schedule was designed and used within all simulations (Fig. 5). The total volumes of fluid and proppant injected were designed to match those planned at well PNR-1Z (400 m^3 and 50 t respectively). The slurry rate was set to 4 m^3/min (again, similar to that used at well PNR-1Z), which results in the desired 400 m^3 of fluid being injected within 100 min (Fig. 5). The proppant concentration was ramped from 0 to 250 kg/m^3 (Fig. 5: proppant concentration), with stepped increases about every 10 min which resulted in the desired 50 t (50,000 kg) of proppant being injected at the end of the treatment (Fig. 5: cumulative slurry).

3.4. Horizontal well design

For the lateral simulations, three horizontal pseudo-wells were side-tracked from the main well PH-1; targeting the three landing zones defined in Part 1 of this series (de Jonge-Anderson et al., 2021b). The pseudo-wells were simplistic in design, with the kick-

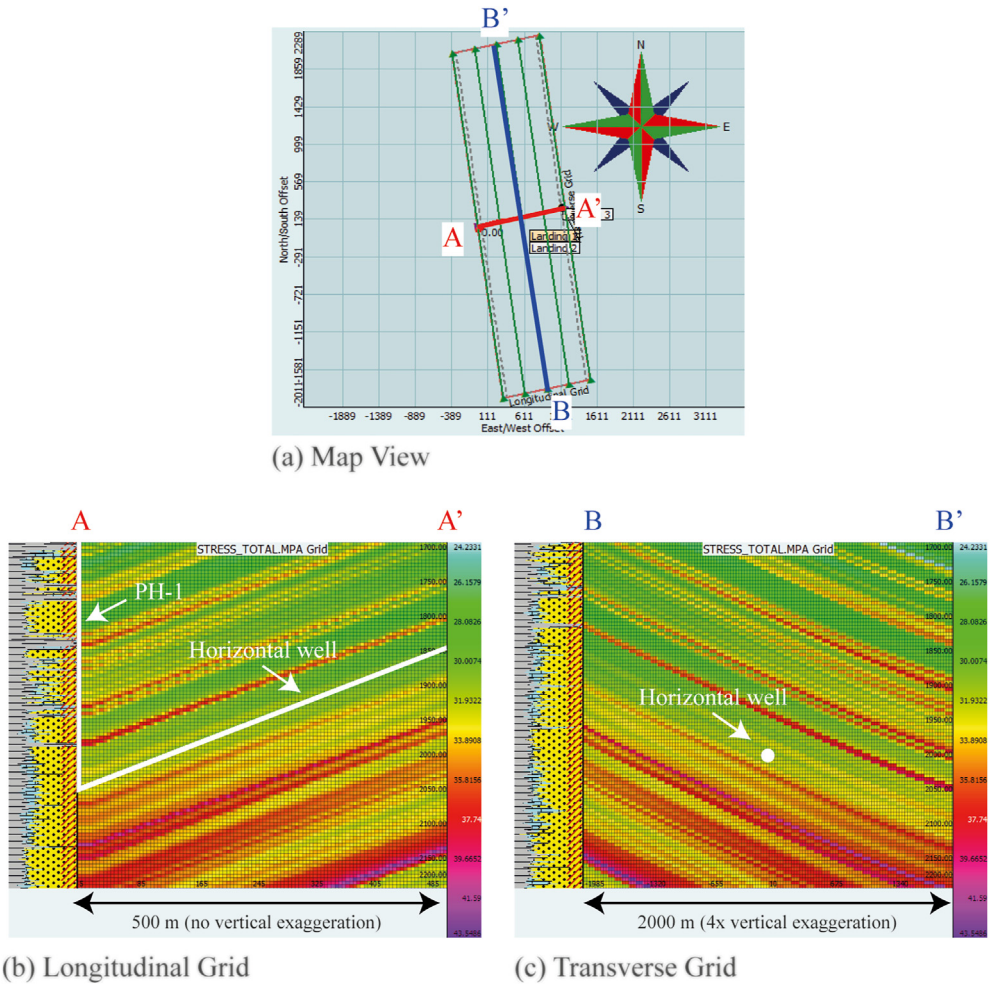

Fig. 4. Illustrations of the GOHFER grid for the lateral simulations where angled, horizontal wells are used, and beds are dipping. (a) Map view showing the extent of the transverse and longitudinal grids relative to a horizontal well trajectory shown in red. (b) Plane view along the longitudinal axis showing the upscaled and gridded total stress and an inclined, horizontal well. (c) Plane view along the transverse axis. Note that (c) is vertically exaggerated by four times, accentuating the angle of dip.

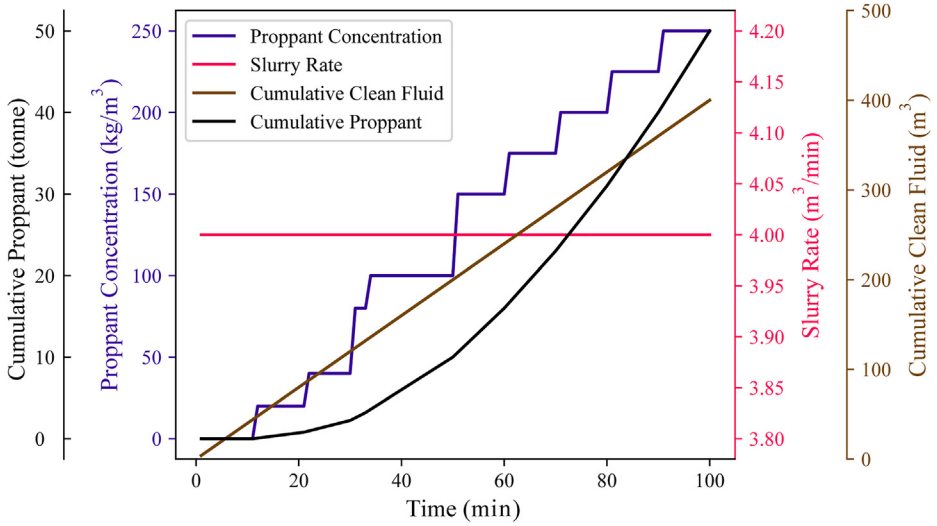

Fig. 5. Illustration of the pumping schedule used for all hydraulic fracture simulations. The schedule was designed based on the planned treatments at well PNR-1Z whereby 400 m^3 of fluid and 50 t of proppant were pumped into each completion stage. Proppant concentration ramps from 0 to 250 kg/m^3 with the slurry rate fixed at 4 m^3/min.

off point taken at the depth of the relevant landing zone and then the horizontal section angled immediately at 20° to follow the bedding orientation. Such a design created a sharp angle with the vertical wellbore (e.g., Fig. 4b) that is unrealistic for any drilling scenario, but all perforation clusters were placed away from this section of the well. Following this, 41 perforation clusters were placed at 12 m intervals along the well (Fig. 6) to mimic the sliding-sleeve design used at PNR-1Z. For the vertical simulations, the same treatment schedule, perforation interval and densities were used; however, clusters were placed at different stratigraphic intervals.

4. Results: vertical simulations

4.1. Testing a selection of geomechanical intervals

A series of simulations were undertaken to model hydraulic fractures within different geomechanical intervals at well PH-1. The first simulation involved modelling perforation clusters at different stratigraphic interval within the Upper Bowland Shale (UBS) (Fig. 7). Perforations were simulated at three possible landing zones (de Jonge-Anderson et al., 2021b), two possible fracture barriers and an intermediate zone of poor completion quality (CQ). An interval with poor CQ exhibits high effective stress, high fracture toughness and low brittleness index (de Jonge-Anderson et al., 2021b). The plot also presents logs of upscaled effective stress and crack density (a proxy for the density of natural fractures; please refer to de Jonge-Anderson et al. (2021a) for further information on calculating crack density).

Hydraulic fractures of varying complexity were simulated and their geometry is highly sensitive to small changes in effective stress within the vertical section. The hydraulic fracture within Landing 1 is narrow, long (up to 1500 m) with its height limited by an interval of slightly elevated effective stress at 2040 m. By contrast, only narrow fractures were simulated at Barriers 1 and 2 and the main fractures instead switched to nearby zones of low effective stress. At Barrier 1, while a very high effective-stress interval above the perforations does not fracture, it appears that stress has transferred across it to form a fracture in the interval above.

Whilst the hydraulic fracture modelled at Landing 3 exhibited a similar character to that of Landing 1, Landing 2 exhibited a more complex geometry. A thin fracture was simulated at the base of the perforated section. This appeared to correlate well with the highest crack density value (0.05) in the section, suggesting that this layer is capable of being fractured. A layer of high effective stress and low/medium crack density at 2275 m appeared to act as a baffle to fracture development and a larger fracture was simulated immediately above the perforated interval (within the good CQ interval that is also accompanied by high, but variable crack densities). The upper portion of the simulated fracture is shorter than the Landing 1 and 2 fractures, propagating about 600 m away from the well.

These simulations provided an insight into the heterogeneity in hydraulic fracture behaviour across the Bowland Shale section at well PH-1. These suggest that the intervals picked for Landings 1 and 3 are producing a good response, characterised by simple, contained fractures; meanwhile, the position of Landing 2 needs to be re-evaluated and moved up to the interval at 2260 m which was modelled to fracture more readily compared with the original target at 2285 m.

4.2. Presence of stress barriers

Effective-stress barriers are key in containing hydraulic fractures and avoiding well-to-well interference in a placement strategy involving stacked horizontal wells. The extent to which high stress intervals within the Bowland Shale can limit hydraulic fracture propagation was tested in two further simulations (Figs. 8 and 9). In each case, a series of perforations were modelled at 20 m separations covering the interval above the fracture barrier, the barrier itself, and the interval below the barrier.

The modelling results suggested that both intervals tested would likely form a barrier to fracture propagation. Tall fractures were modelled within the perforated intervals located above the first fracture barrier (Figs. 8 and 9). Where perforations were modelled at the top of the fracture barriers, no fracture formed in the barrier itself and the fracture instead propagated in adjacent intervals. Where the intervals below the barriers were perforated, the main fractures formed in the region of the perforation, with few growing up into the barrier.

5. Results: lateral simulations

The following section describes the results of simulations performed along horizontal pseudo-wells that targets three landing zones within well PH-1. While hydraulic fractures were simulated for all 41 clusters; in many cases only the first five are shown. The geological grid used as input was tilted to create a scenario more representative of the dipping stratigraphy east of well PH-1 (Fig. 4). The simulations were designed to assess the impact of stress shadowing along the horizontal pseudo-well, the modelled transverse fracture geometry and the spatial extent of modelled fractures.

5.1. Stress shadowing

A simulation was first designed to investigate the impact of stress shadowing on two perforation clusters placed 12 m apart, whilst testing a range of transverse exponent values between 1.2 and 2 (Fig. 10). The results suggest that the stress shadowing effect has a significant impact on hydraulic fracture geometry for perforation clusters placed 12 m apart and stimulated consecutively. Whilst using a transverse exponent of 2 leads to a negligible difference in modelled fracture geometry between Cluster 1 and

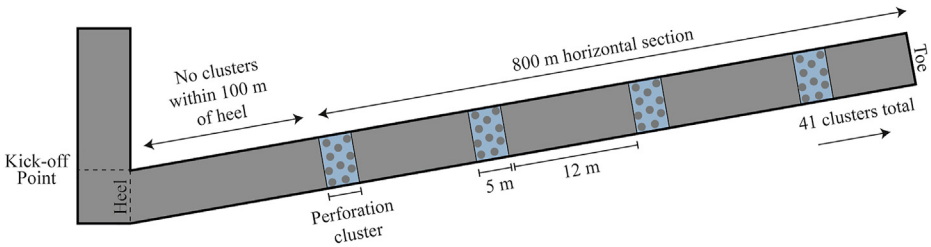

Fig. 6. Illustration of the plug-and-perf completion design for each pseudo well, adapted from the sliding sleeve design used at PNR-1Z. The pseudo-wells were inclined to 20° to track the bedding dip to the east of well PH-1. For simplicity, no building section was included and the lateral kicked-off at a sharp angle from the main vertical well. 41 perforation clusters were placed along the horizontal section, each of 5 m long and with 12 m interval.

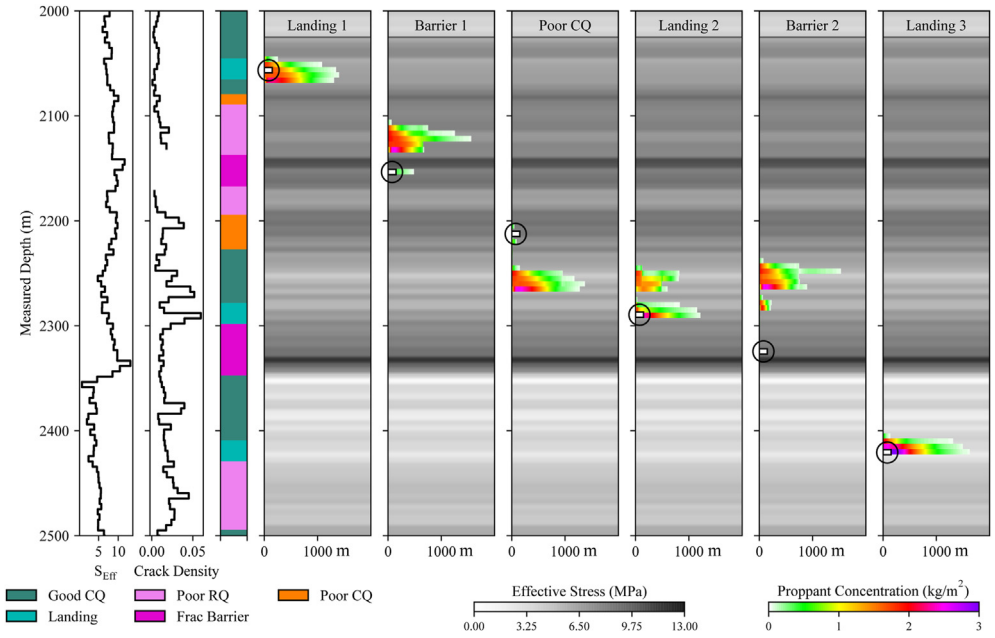

Fig. 7. Results of a vertical hydraulic fracture simulation plotted next to a selection of input logs for a section of the UBS between 2000 and 2500 m in depth. Six intervals were tested: three landing zones, two potential barriers and an interval of poor Completion Quality. Completion Quality (CQ) and Reservoir Quality (RQ) intervals were defined in de Jonge-Anderson et al. (2021a) and de Jonge-Anderson et al. (2021b), respectively. The perforated interval is shown as the white box with a black circle outline. While Landings 1 and Landings 3 exhibit simple fracture geometry, Landing 2 exhibits a more complex fracture consisting of two individual fractures. For the remaining perforations, fractures are poorly developed within the perforated zone, as expected. Effective stress, shown in track 1, is calculated as closure stress minus pore pressure and inverted crack density is shown in track 2. Both are upscaled to the simulation grid scale.

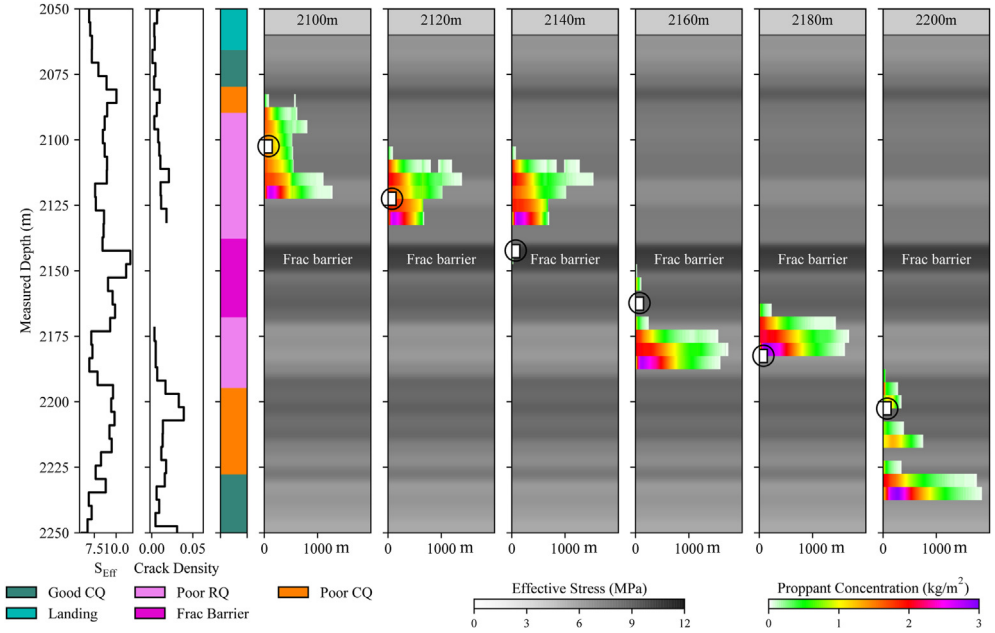

Fig. 8. Results of a vertical hydraulic fracture simulation designed to test the containment of hydraulic fractures by a potential fracture barrier highlighted at 2150 m. In each case, the perforated interval is shown as a white box with a black circle outline. The depth of each interval is highlighted at the top of the corresponding panel. The results suggest that the interval is efficient in halting hydraulic fracture propagation as there is almost no propagation within the highly stressed zone. There is, however, a small fracture that develops at the base of the interval (e.g., at the 2160 m perforation). Effective stress, shown in track 1, is calculated as closure stress minus pore pressure and inverted crack density is shown in track 2. Both are upscaled to the simulation grid scale.

Cluster 2 (Fig. 10; top row), decreasing the exponent led to an increase in the minimum horizontal stress region around the second cluster, and in extreme cases, led to the Cluster 2 hydraulic fracturing propagating in a different orientation to that in Cluster 1 (Fig. 10; bottom two rows).

These models suggest that the stress shadowing effect is profound when perforation clusters are placed 12 m apart within a unit of geomechanical properties representative of the Bowland Shale. This observation is supported by some field evidence collected during the hydraulic fracturing of well PNR-2 whereby a switch in

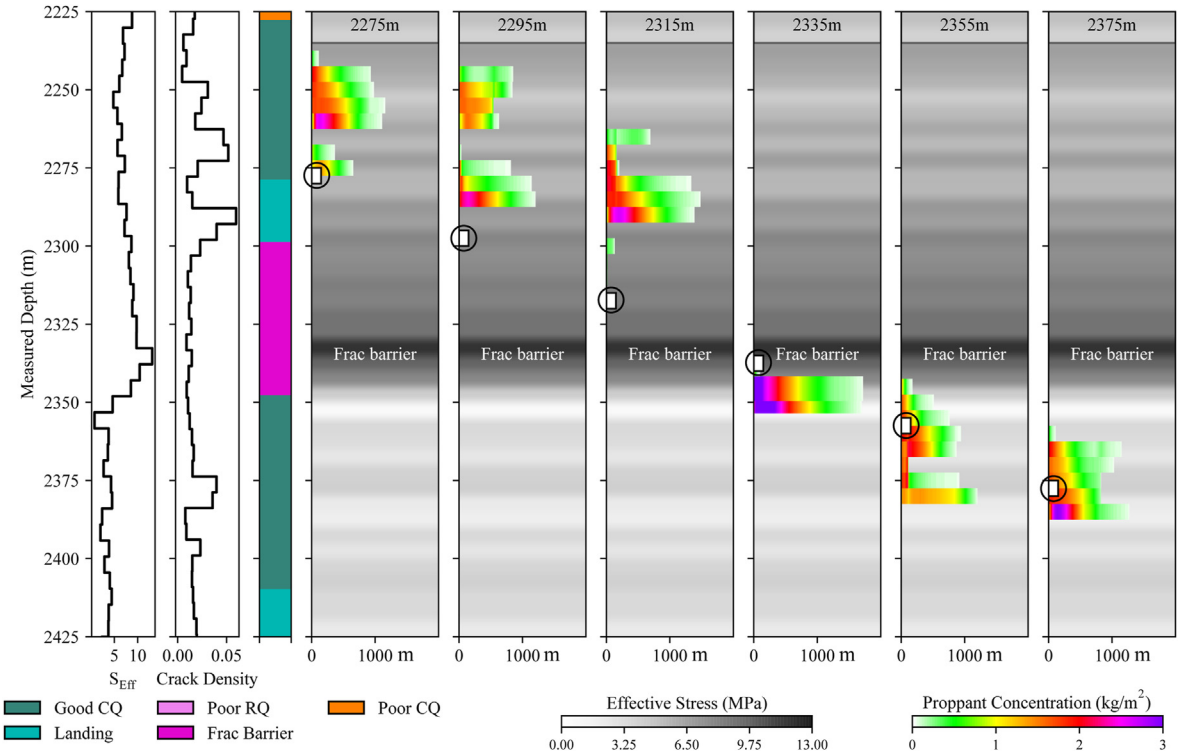

Fig. 9. Results of a vertical hydraulic fracture simulation designed to test the containment of hydraulic fractures by a potential fracture barrier highlighted at 2325 m. In each case, the perforated interval is shown as a white box with a black circle outline. The depth of each interval is highlighted at the top of the corresponding panel. The results suggest that this interval is also efficient in halting hydraulic fracture propagation as there is almost no propagation within the highly stressed zone. Effective stress, shown in track 1, is calculated as closure stress minus pore pressure and inverted crack density is shown in track 2. Both are upscaled to the simulation grid scale.

hydraulic fracture propagation direction between adjacent stages has been linked to the effects of stress shadowing (Verdon et al., 2020).

5.2. Fracture geometry

Multi-stage simulations were then conducted along each horizontal pseudo-well to determine the fracture height, length and proppant distribution of each stage. For Landing 1 (Fig. 11), narrow and long fractures were modelled. All fractures were dipping; tracking the dipping beds and geological grid used as input to the simulations. A high effective stress layer contained the fractures in all cases, with the main fracture forming between the perforations and this barrier. In several instances (stages 1, 2, 4 and 5), the fracture appeared to form as two separate fractures separated by a small baffle, whereas in stage 3 a fracture only developed in the upper zone.

The effect of stress shadowing on simulated fracture geometry was also observed. While the stage 1 fracture propagated south, stage 2 propagated north. Both stage 2 and stage 3 propagated north, and seemingly the stress increase owed to the hydraulic fracture width in this region served to limit fracture development in that region by stage 4. This asymmetric pattern created complex fracture patterns that if observed in the field, would not be desirable.

The simulated fractures from Landing 2 (Fig. 12) exhibits more consistent geometry. The main fracture propagated up from the perforations and then laterally within a unit of lower effective stress than surrounding layers. In all instances, the simulated fracture was more symmetrical than observed in Landing 1, though the fracture did extend farther south than north. The stress shadow effect did not appear to significantly alter the fracture geometry, though a more irregular proppant distribution was observed in later clusters (i.e., 2, 3, 4 and 5) compared to Cluster 1. The modelled fractures were narrow, appearing to be contained by the high effective stress unit 25 m above the perforations, and propagating around 1000 m from the well.

The simulated fractures from Landing 3 (Fig. 13) exhibited complex geometry as a result of stress shadowing. While Cluster 1 simulated a simple fracture that propagated upwards from the perforations and then laterally, as confined by the high effective stress layer about 30 m above, the fractures within subsequent clusters are more complex. For Clusters 2 and 3, several intervals formed baffles to fracture development, the modelled fractures in stacked, smaller pattern were observed in contrast to the single fracture modelled in Cluster 1. By Cluster 4 the main fracture appeared to propagate south, followed by no fracture development in this area by Cluster 5.

The results of the above simulations are also shown for all 41 perforation clusters in map view (Fig. 14). Most modelled fractures were about 600 m in half-length for all landings, but the longest (up to 1100 m) were observed within Landing 3. Hydraulic fractures simulated at this landing ranged from 375 m to 1100 m in half-length and the longest fractures appeared to be simulated nearest to the heel of the well. Landings 1 and 2 showed similar ranges of fracture extent and were shorter than those observed in Landing 3. The fracture half-lengths at Landing 1 ranged between 410 m and 700 m and those of Landing 2 between 448 and 738 m. Differences in the distribution of proppant within each landing zone were also observed. In Landing 2, most of the proppant was placed within an interval near to the well (<100 m); while in Landing 3 the proppant was even more widely distributed, with high concentrations up to 500 m away from the well.

The total formation area covered by all the fractures was also determined. A simplistic approach was followed whereby the

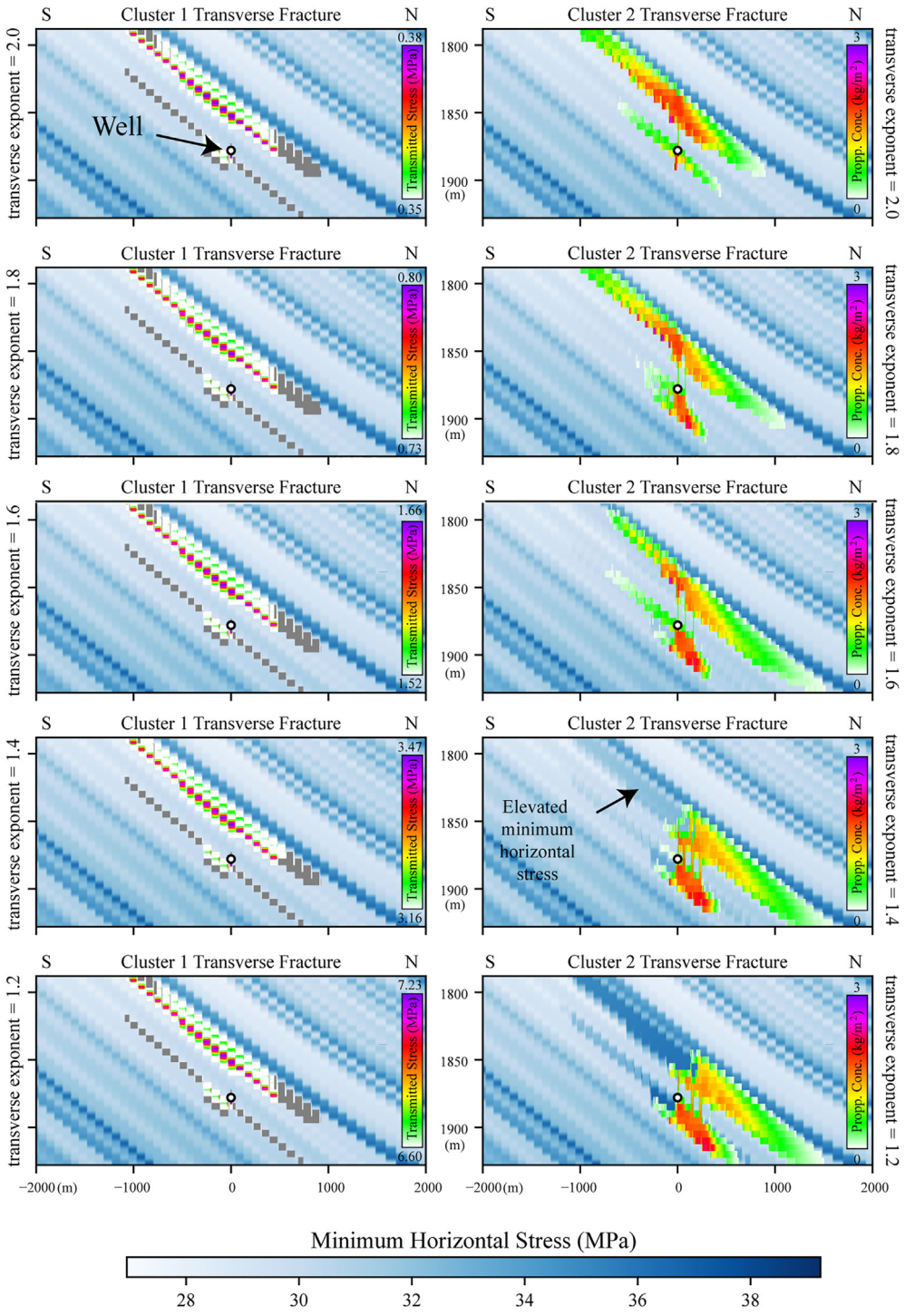

Fig. 10. A series of transverse fracture simulations highlighting the impact of the transverse exponent on the stress shadow effect between two closely spaced perforation clusters. Each row of panels represents a simulation using a given transverse exponent. The background blue shading shows the minimum horizontal stress of the rock in which the hydraulic fracture is propagating. The simulated fracture in the left panel shows the geometry of the Cluster 1 transverse fracture, coloured by its transmitted stress. The simulated fracture in the right panel shows the Cluster 2 fracture, accounting for the stress shadow from Cluster 1 and with shading corresponding to proppant concentration.

fracture length was multiplied by the grid size (5 m) to calculate the area covered per fracture. These were then summed to produce a final area stimulated per fracture. Following this approach, the fracture areas for Landings 1, 2 and 3 were determined to be 0.227 km^2, 0.240 km^2 and 0.245 km^2, respectively. Table 2 summarises the fracture half-lengths and areas above in addition to quoting them using a 2 kg/m^2 proppant cut-off for comparison.

5.3. Fracture extents and major faults

The results of the simulations described previously can be used to further understand the limits placed by the structural features described by de Jonge-Anderson and Underhill (2020). This can be assessed in two parts; firstly, addressing how close a completion stage can be placed near to a major fault without risk of interfering

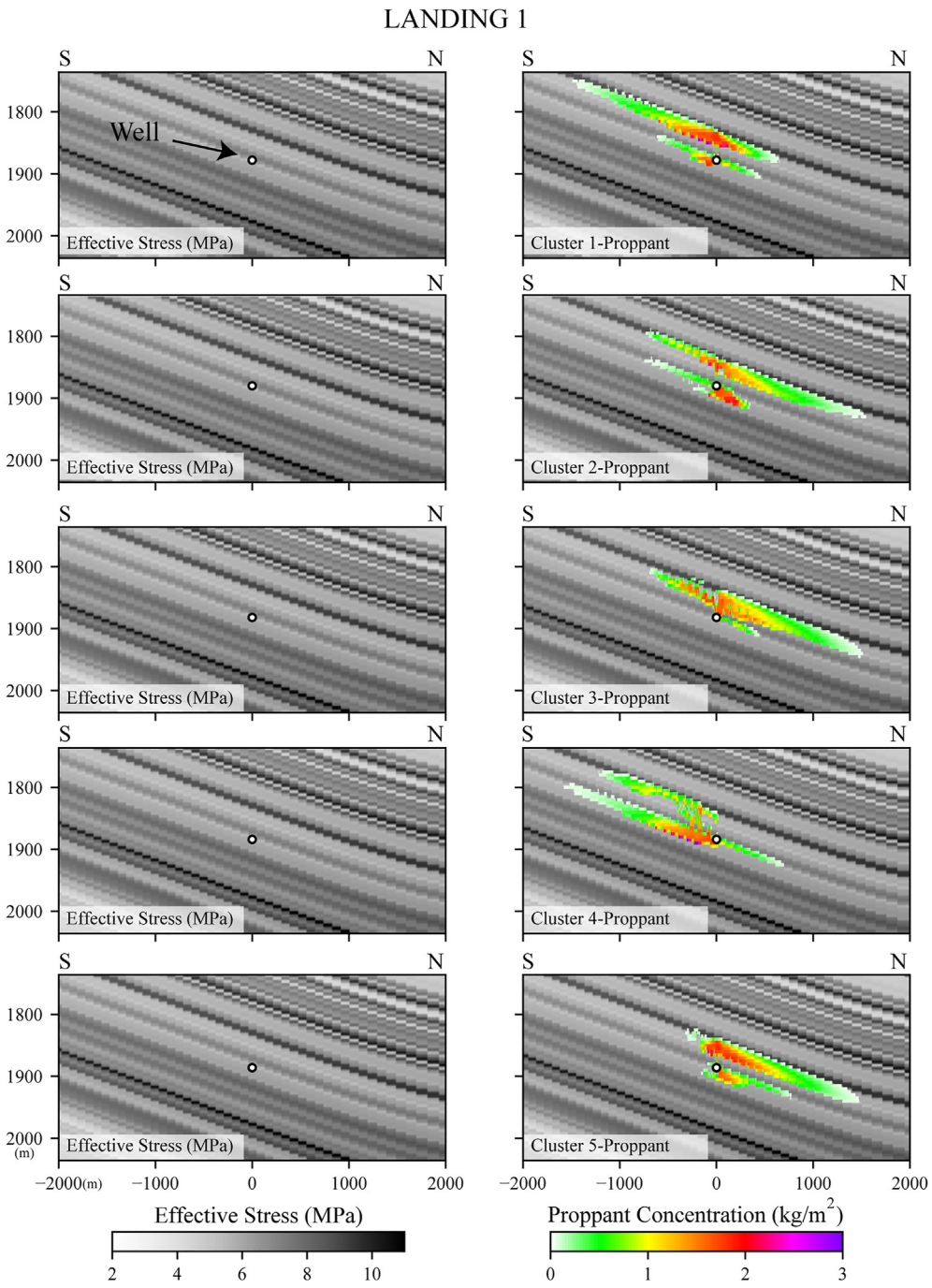

Fig. 11. Modelled transverse fractures for five perforation clusters along Landing 1. For each cluster, the effective stress grid (left) and modelled proppant distribution within the fractures (right) are shown. Each row represents a cluster (the first five clusters) and for each cluster, the simulated proppant distribution within that fracture is shown on the right column. In each case, a transverse fracture is shown along the plane of maximum horizontal stress (the transverse grid, shown in Fig. 4), centred on the perforation and with north to the right.

hydraulic fractures with said fault; and secondly, studying where within the 100 km^2 study area there is potential for other wells to be drilled.

5.3.1. Positioning stages

To quantify the distance from major faults that completion stages can be placed for the Bowland Shale in this area, two scenarios are envisaged. Each scenario corresponds to a different effective fracture length, determined by taking a cut-off as to the maximum concentration of proppant within the fracture. Proppant placement within a fracture is considered a proxy for the likelihood of it generating microseismic events at that location. Some studies suggested that microseismic activity peaks at the onset of proppant placement in a stimulation (McKenna, 2014); however, it is challenging to determine at what concentration a fracture is sufficiently pressurised and propped to pose a risk to geological structures. To attempt to express this uncertainty, two cut-offs of proppant concentration were taken, which in turn correspond to two effective fracture lengths.

In the first scenario (Scenario A), an effective fracture is considered where proppant concentrations exceed 1 kg/m^2.

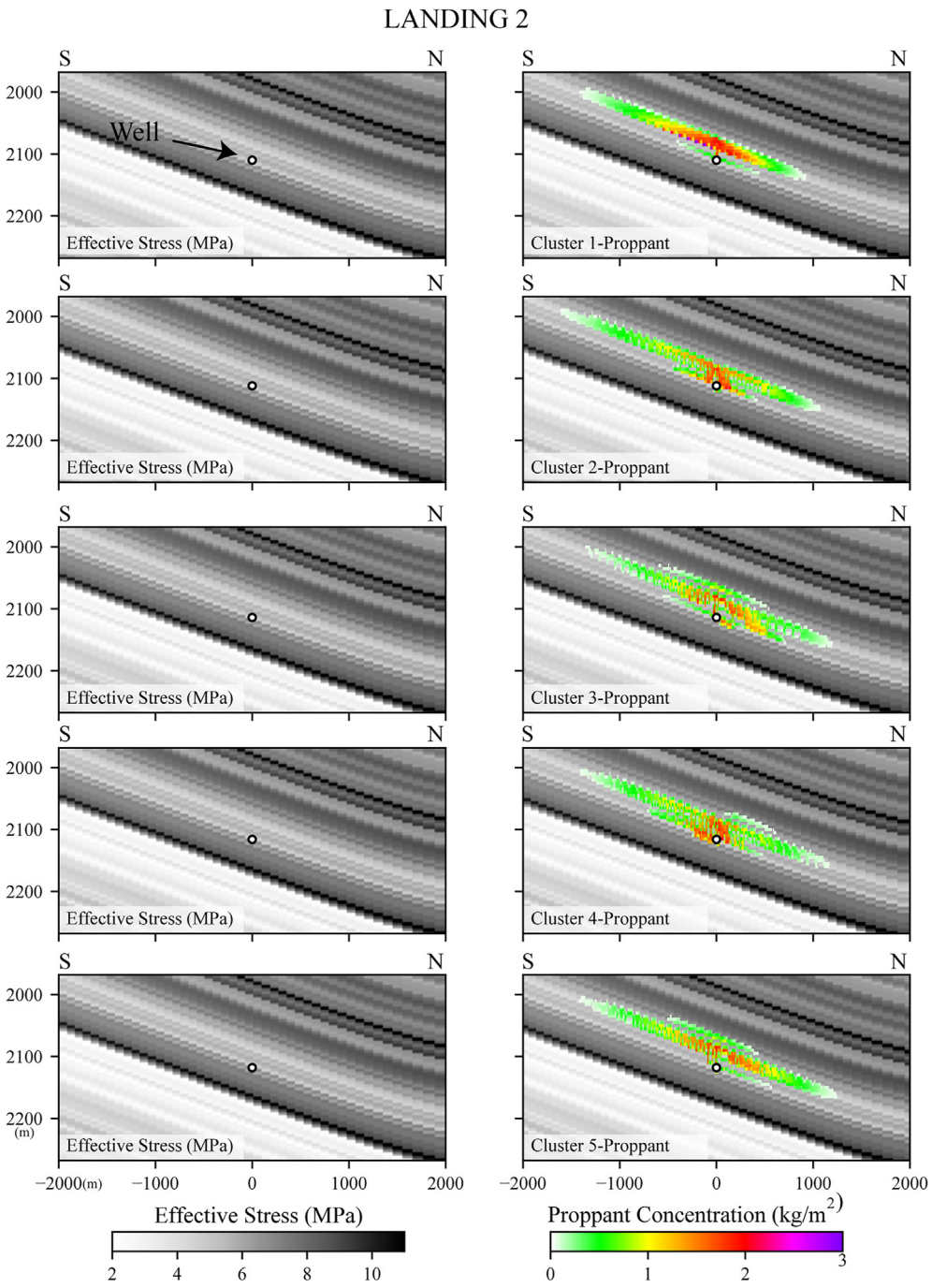

Fig. 12. Modelled transverse fractures for five perforation clusters along Landing 2. For each cluster, the effective stress grid (left) and modelled proppant distribution within the fractures (right) are shown. Each row represents a cluster (the first five clusters) and for each cluster, the simulated proppant distribution within that fracture is shown on the right column. In each case, a transverse fracture is shown along the plane of maximum horizontal stress (the transverse grid, shown in Fig. 4), centred on the perforation and with north to the right.

Observing the maximum fracture lengths for this cut-off (Fig. 14; Table 2) reveals that Landing 3 holds the longest maximum fracture half-length (1100 m), which is significantly greater than the other landings (about 750 m of maximum half-lengths). In the second scenario (Scenario B), an effective fracture is considered whereby proppant concentrations only exceed 2 kg/m^2. Where the maximum length measured accounts for this cut-off (Table 2), Landing 3 again holds the longest maximum fracture half-length (545 m), though it is substantially smaller than for Scenario A.

A simplified version of the map presented in Fig. 2 is presented for both scenarios (A-upper and B-lower) (Fig. 15). A lateral well was side-tracked from well PH-1 along the azimuth of minimum horizontal stress as far as the Moor Hey Fault. In Scenario A, no stages can be placed along 1800 m of the lateral well without the risk of the northward-propagating fractures interfering with the Summerer Fault. Similarly, no stages can be placed within the last 1230 m of the horizontal section without the risk of southward-propagating fractures interfering with the Moor Hey Fault. Consequently, there is a 400 m section of the lateral well (shaded in red) where hydraulic fracture stages could be placed with minimal risk.

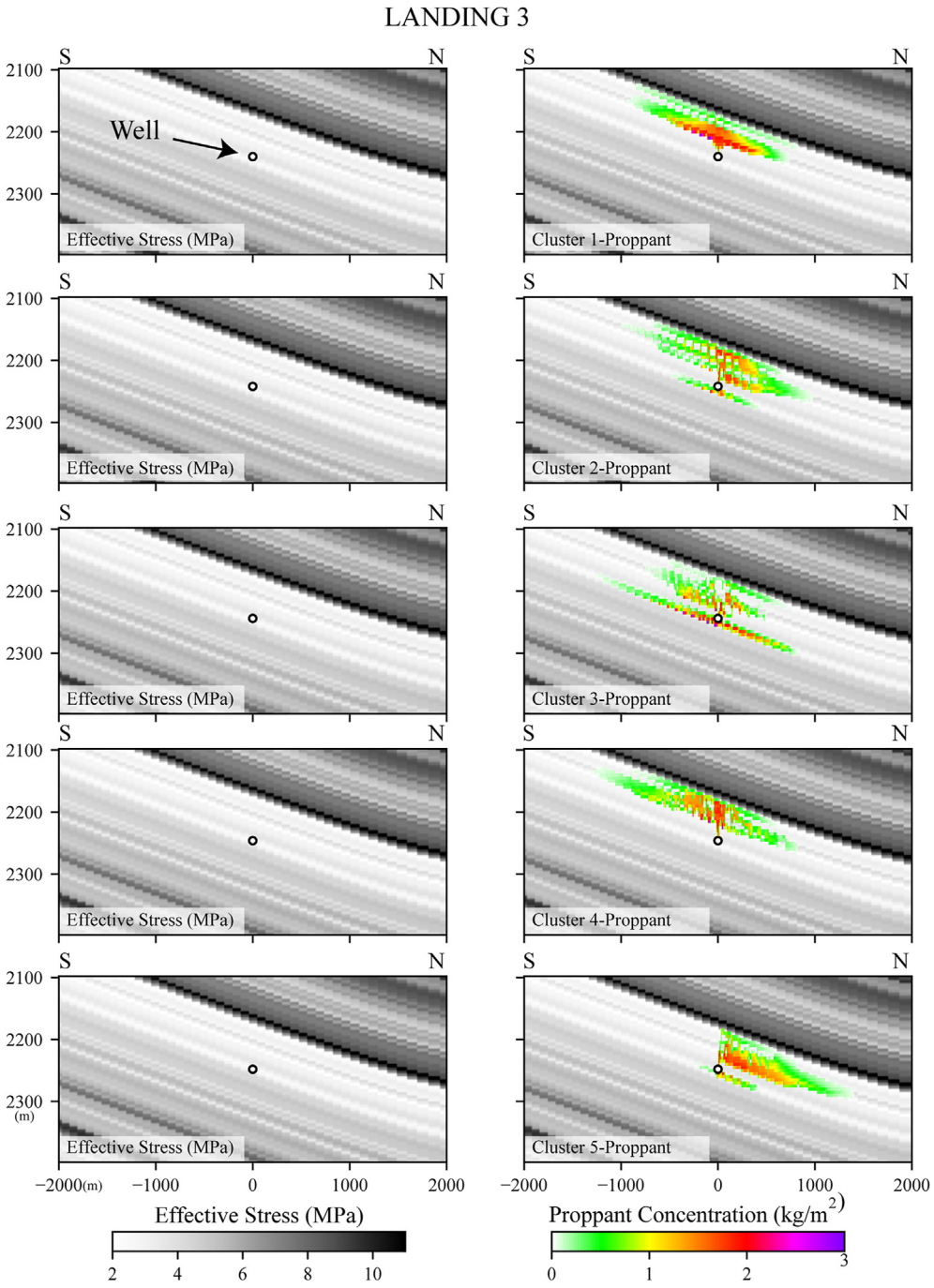

Fig. 13. Modelled transverse fractures for five perforation clusters along Landing 3. For each cluster, the effective stress grid (left) and modelled proppant distribution within the fractures (right) are shown. Each row represents a cluster (the first five clusters) and for each cluster, the simulated proppant distribution within that fracture is shown on the right column. In each case, a transverse fracture is shown along the plane of maximum horizontal stress (the transverse grid, shown in Fig. 4), centred on the perforation and with north to the right.

This suggests that using this scenario, drilling pilot wells at the edge of the fault blocks may not be the optimal approach as over 1800 m of deviated section is needed before a hydraulic fracturing stage can be placed. Instead, the wells should be placed more centrally within the block and with short horizontal sections. Smaller faults such as that to the immediately south-east of well PH-1 and that to the west of the Moor Hey Fault are not considered in this part of the analysis.

In Scenario B, a 1900 m section of the lateral well can be stimulated (red shading) without risk of the shorter effective fractures encountering the Summerer and Moor Hey Faults. Near the heel, no stages can be paced in the first 870 m without risking northward interference with the Summerer Fault, and likewise, no stages can be placed within the last 615 m of the well, near the toe. In this scenario, a well placed near the edge of the block can still provide a useful vertical well from which to side-track horizontal sections, however, a deviated section of around 500–1000 m is needed before hydraulic fracturing stages can be placed on the horizontal section.

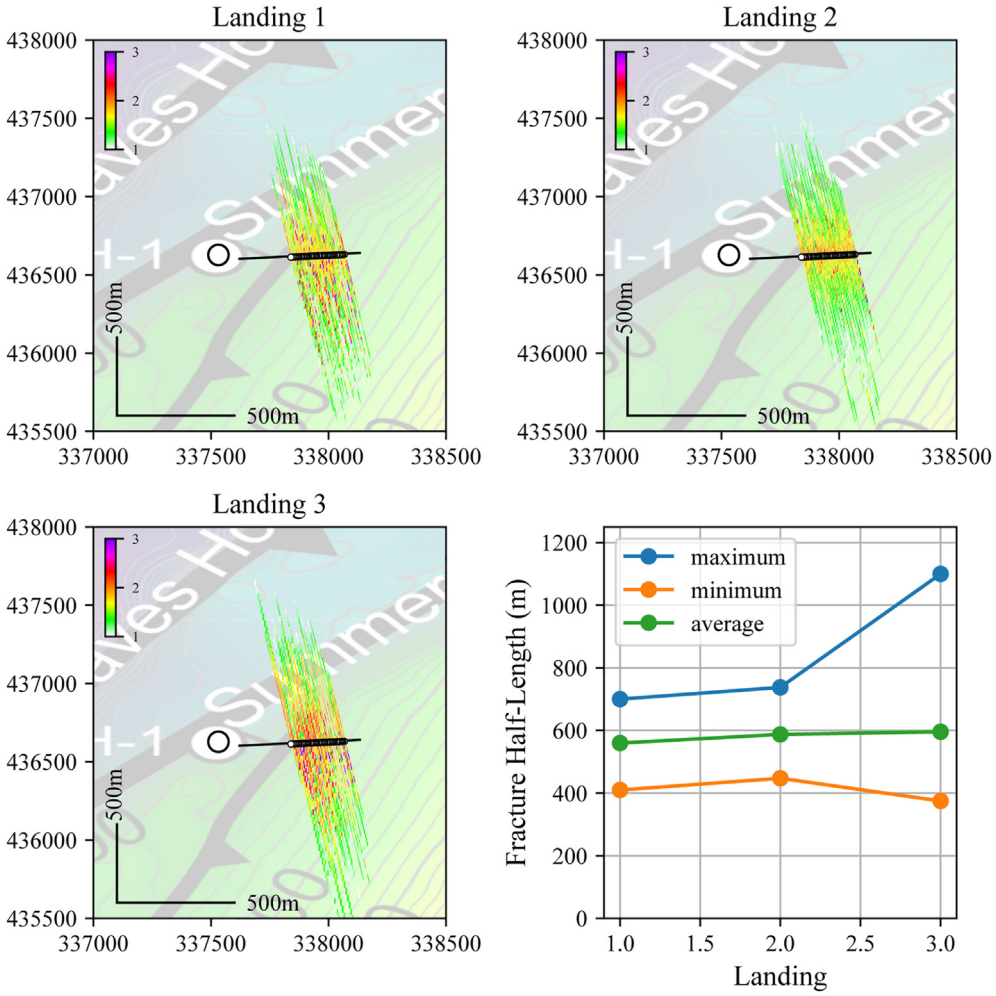

Fig. 14. Maps illustrating the spatial extent of modelled fractures and a line graph showing the maximum and minimum length (assuming a proppant concentration of 1 kg/m^2) of modelled fractures for each well. In the map views, the maximum proppant concentration (for all depths) was calculated for each X–Y location along the fracture and is represented as a single colour value. Note that the X and Y scales are not equal and so the azimuths of well trajectory and fracture propagation may not reflect their true orientations. The location of the map is shown in Fig. 1.

Table 2
A summary of fracture half-lengths and areas for the three landing zones and quoted using both a 1 kg/m^2 proppant concentration cut-off and a 2 kg/m^2 cut-off. These are referred to as Scenarios A and B.

		Landing 1	Landing 2	Landing 3
1 kg/m^2 cut-off	Min. half-length (m)	410	448	375
	Max. half-length (m)	700	738	1100
	Area (km^2)	0.227	0.240	0.245
2 kg/m^2 cut-off	Min. half-length (m)	5	5	15
	Max. half-length (m)	428	368	545
	Area (km^2)	0.082	0.053	0.093

5.3.2. Well placements in the area

The final objective of the study is to consider the implications of these typical fracture geometry not just for the region near well PH-1, but for the region mapped using the Bowland-12 seismic survey (Fig. 2). Specifically, it seeks to determine where lateral wells could be emplaced without hydraulic fractures interfering either with fractures from adjacent wells or significant structural features such as faults.

For this, it was assumed that all fractures are symmetrical, with the lateral well forming the axis of symmetry and with all fractures the same length. As a result, the overall footprint then becomes a rectangle, centred on the lateral well and rotated such that the well trajectory is parallel to minimum horizontal stress. The trajectory of the well is not explicitly considered, and the heel could be emplaced in the ENE or WSW of the lateral section. Two scenarios are considered, corresponding to 1 kg/m^2 and 2 kg/m^2 proppant cut-offs (Figs. 16 and 17 respectively). The placements are made based solely on the subsurface information contained in the map; though in reality, surface constraints such as environmental concerns and other subsurface constraints such as good quality seismic reflectivity will also guide well placement.

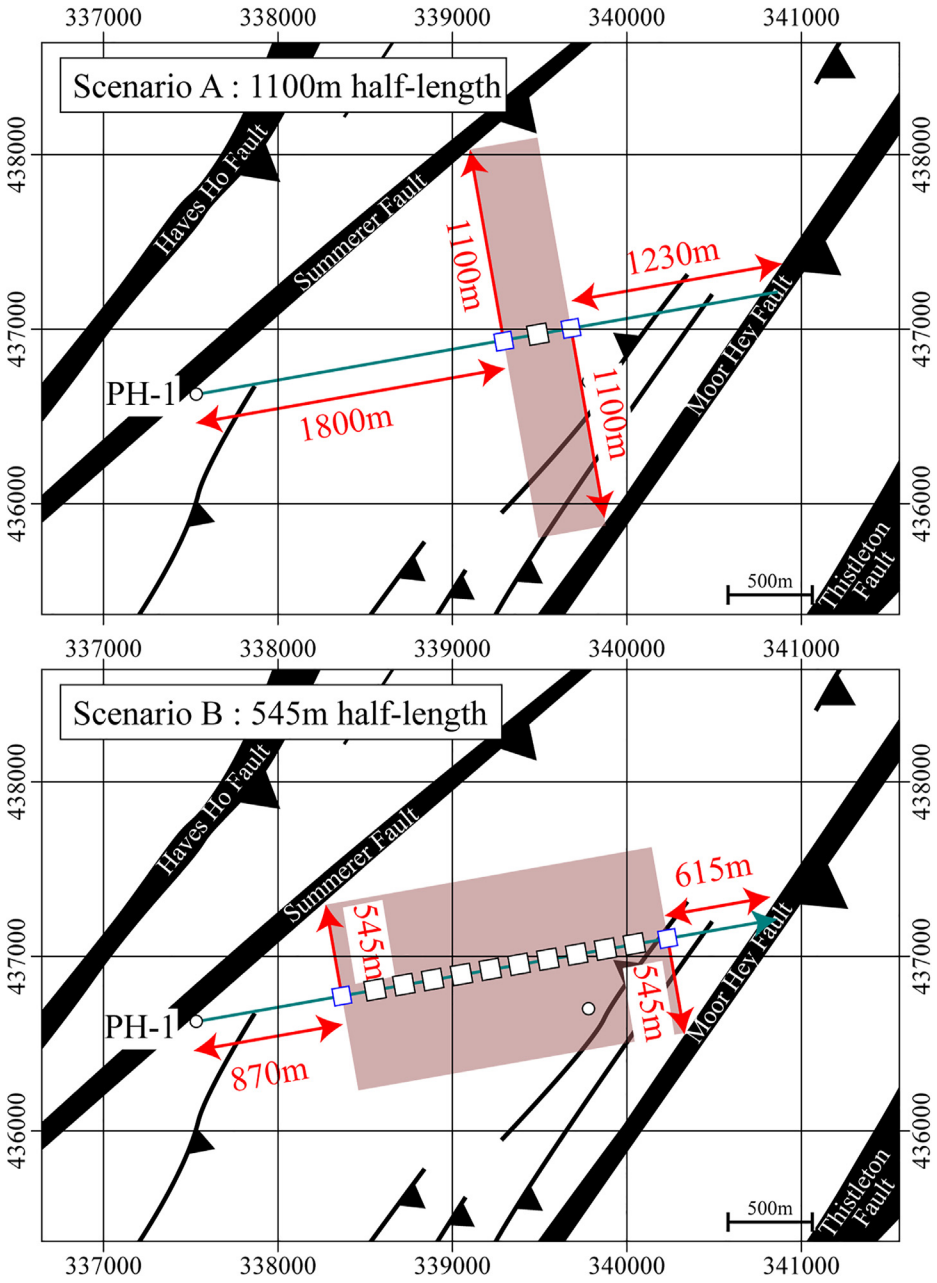

Fig. 15. Maps illustrating the distance from major faults that need to be kept to avoid hydraulic fractures interfering with said faults. The location of the maps is shown in Fig. 1. Two scenarios corresponding to two different fracture lengths are presented. In the upper map (Scenario A), an effective fracture is considered where the proppant concentration is greater than 1 kg/m^2 and thus the maximum fracture half-length is 1100 m. In the lower map (Scenario B), an effective fracture is considered where the proppant concentration is greater than 2 kg/m^2 and thus the maximum fracture half-length is 545 m.

Using a 1100 m half-length, few sites can accommodate a lateral well without fractures intersecting significant (seismic scale) faults (Fig. 16). The Poulton Block in the NW corner can accommodate a 1.3 km long lateral well, though approaches the limit of the Bowland-12 3D survey. The Singleton Block is too narrow to accommodate a well without fractures intersecting either the Haves Ho or Summerer Fault. The Weeton Block is the widest in the region to the immediately south of well PH-1 and near the PNR wells. In this area, a 0.9 km long lateral can be achieved. The trajectory is placed slightly further north than the current PNR location to avoid south-propagating fractures interfering with the Anna's Road Fault. Between this location and well PH-1, a shorter, 0.7 km lateral can be achieved, but its easterly limit is restricted by a series of small reverse faults near to the larger Moor Hey Fault. As the Weeton Block narrows to the north of well PH-1, it becomes impossible to accommodate a lateral well using this cut-off without intersecting either the Summerer Fault or the aforementioned reverse fault zone immediately west of the Moor Hey Fault. While the focus of this work has been in the footwall to the Thistleton Fault, where the overlying Permo-Triassic sequences are less developed, two lateral wells were placed in the Elswick Graben hanging-wall. Two longer wells (1.4 km and 1.2 km in length) can be achieved; however, a caveat in emplacing wells in this location is the uncertainty in the mapping of the Carboniferous sequences beneath the thicker Permo-Triassic succession (de Jonge-Anderson and Underhill, 2020). The total area covered by this configuration (calculated as lateral length multiplied by fracture length) is 12.1 km^2.

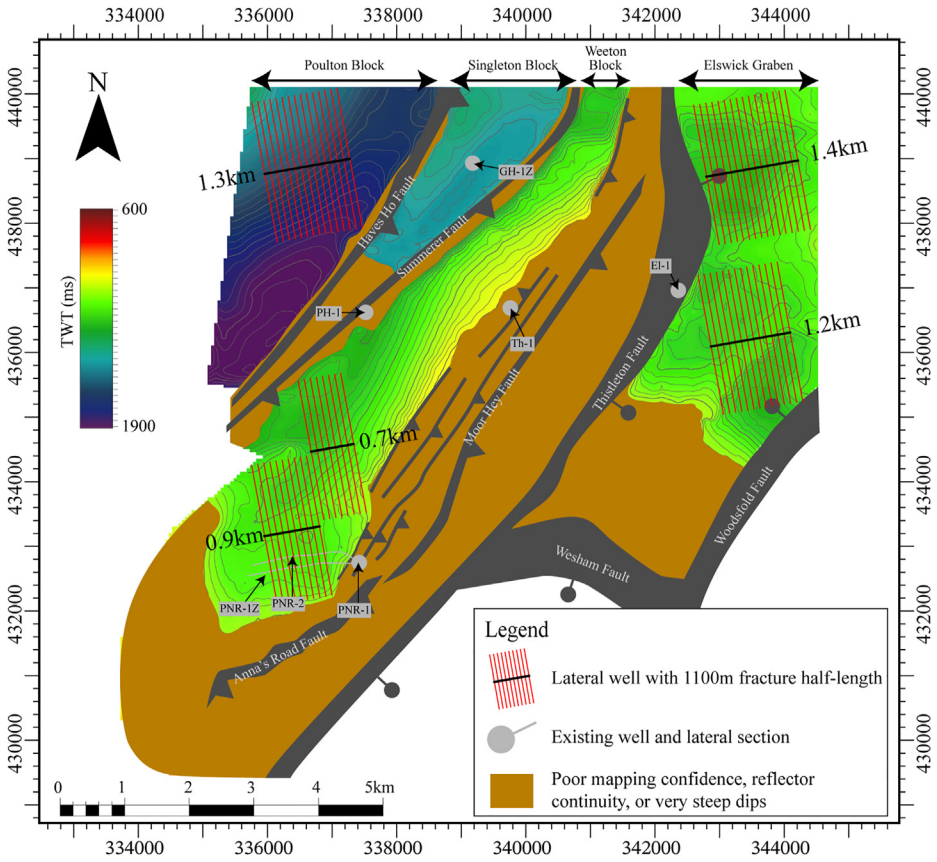

Fig. 16. Map highlighting the areas within the Bowland-12 survey that lateral wells could be emplaced without hydraulic fractures interfering with major faults or with hydraulic fractures from adjacent wells. The 1100 m predicted half-length of the hydraulic fractures is taken using a proppant cut-off of 1 kg/m^2. The underlying contour map is the Lower Bowland Shale contoured in two-way time (in milliseconds) (de Jonge-Anderson and Underhill, 2020). The black lines represent the lateral well drilled along minimum horizontal stress orientation and the hydraulic fractures represented as red lines. The brown shading is added where steep dips associated with faulting and folding, or a lack of seismic reflectivity would inhibit drilling.

When the maximum hydraulic fracture length for a 2 kg/m^2 proppant concentration is considered, many more lateral sections can be achieved within the survey area (Fig. 17). In the Poulton Block, the stage closest to the east can be moved closer to the Haves Ho Fault, thus allowing the lateral section to increase in length from 1.3 to 2.3 km before reaching the end of the survey. A further two shorter wells of 1.5 km and 0.7 km in length can be emplaced in the further south of the block. A small lateral of 0.8 km long can now be achieved within the narrow Singleton Block. The Weeton Block can accommodate more lateral wells around well PH-1. These wells are generally short (<1 km in length) as longer ones would risk hydraulic fractures interfering with either the Summerer Fault or the fault zone around the Moor Hey Fault. In the south-west area, the lateral well emplaced north of the current wells PNR -1Z and 2 can reach 1.8 km in length and another well can be set adjacent to this site (1.6 km in length). In the Elswick Graben, four wells can be drilled, reaching 2 km in length, though the caveat to this area discussed earlier remains. The total area covered by this configuration (calculated as lateral length multiplied by fracture length) is 18.9 km^2.

6. Discussion

6.1. Uncertainties in fracture lengths

This work presents forward models for predicting hydraulic fracture geometry using a calibrated geological model for the state of stress in the subsurface, before drilling and stimulating horizontal production wells. Planar fracture models are popular tools in the unconventional industry but are a simplistic representation of how hydraulic fractures propagate in the subsurface and this drawback is becoming increasingly supported by field studies of stimulated unconventional reservoirs. Studies of the Eagle Ford Shale stimulated rock volume have demonstrated that hydraulic fracture propagation is heterogeneous, with many forming in swarms and branching at bedding surfaces (Raterman et al., 2017, 2018, 2019). Analysis of core samples at the Midland Basin Hydraulic Fracture Test Site also revealed complex fracture geometry of diverse types, which are sensitive to the presence of natural fractures (Ciezobka et al., 2018; Gale et al., 2018).

However, in most instances, microseismic events are the only field data available to validate hydraulic fracture characteristics. For the Bowland Shale, such field data has been released for an adjacent well (well PNR-1Z) (North Sea Transition Authority, 2019), and reports discussing the relationship between geomechanical conditions and hydraulic fracture/microseismic behaviour have been published for wells PNR-1Z (Verdon et al., 2019) and PNR-2 (Verdon et al., 2020).

Accurate calibration of fracture models using such data from the wells PNR-1Z and PNR-2 would have required a separate geological model describing the stress and rock properties at that site, and the data required to construct such a model were not available for this study. However, the need to scrutinise the modelling results with field data was also recognised. To that extent, the key findings of the hydraulic fracturing at these sites were discussed, in addition to the implications for the modelling results at well PH-1.

The microseismicity observed following hydraulic fracturing of wells PNR-1Z and PNR-2 has been well documented. In each case,

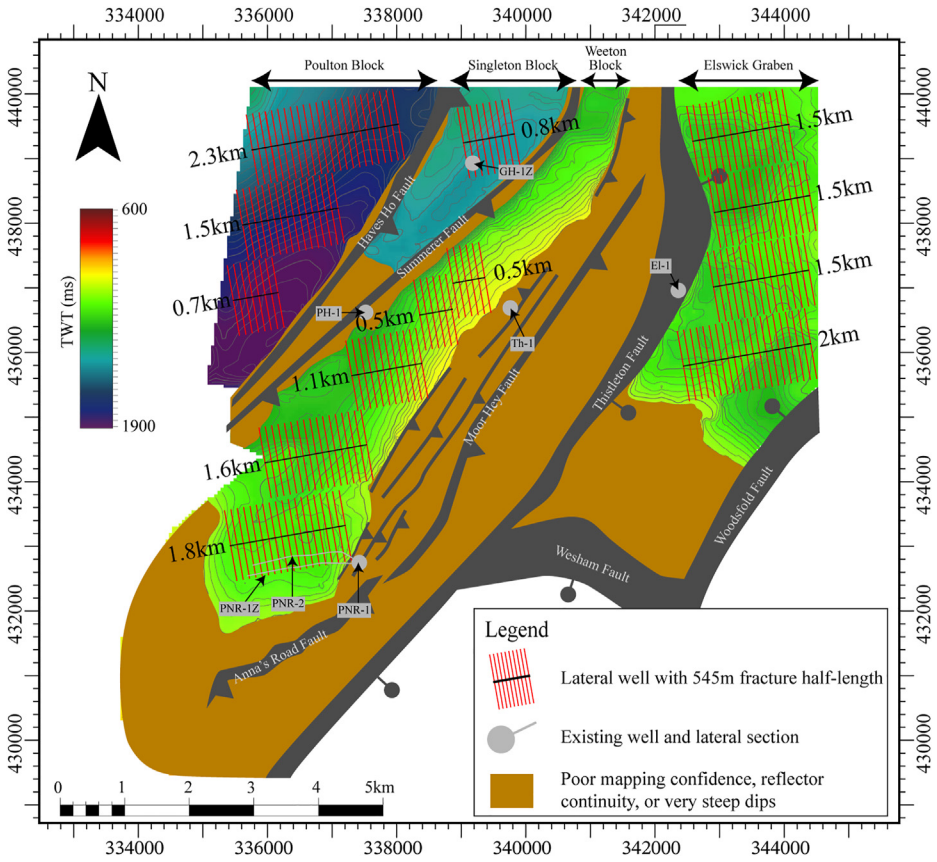

Fig. 17. Map highlighting the areas within the Bowland-12 survey that lateral wells could be emplaced without hydraulic fractures interfering with major faults or with hydraulic fractures from adjacent wells. The 545 m predicted half-length of the hydraulic fractures is taken using a proppant cut-off of 2 kg/m^2. The underlying contour map is the Lower Bowland Shale contoured in two-way time (in milliseconds) (de Jonge-Anderson and Underhill, 2020). The black lines represent the lateral well drilled along minimum horizontal stress orientation and the hydraulic fractures represented as red lines. The brown shading is added where steep dips associated with faulting and folding, or a lack of seismic reflectivity would inhibit drilling.

events were monitored using a combination of surface sensors (seismometers and geophones) and subsurface geophones placed in the adjacent well. At well PNR-1Z, whilst the surface network of sensors identified 54 events, the borehole geophones identified 39,000 events which extended about 200 m north of their corresponding sleeve and around 150 m above and below the well (Clarke et al., 2019b; Verdon et al., 2019). At well PNR-2, significantly more microseismic events were recorded (120 events identified from the surface array and 55,000 events identified using borehole geophones), and the locations of some of those events suggested a hydraulic fracture system extending 350 m north of the well (Verdon et al., 2020). This variability in microseismic pattern and inferred hydraulic fracture character between two adjacent wells suggests a complex subsurface state.

However, in both cases, the microseismic distribution and magnitude was related to the geomechanical failure of faults very near the wells. Clarke et al. (2019b) used the microseismic event distribution at well PNR-1Z to identify a small, sub-seismic-scale fault and Verdon et al. (2020) subsequently identified a separate structure upon which the largest events were recorded at well PNR-2. Such weak geomechanical units will fail readily and strongly influence hydraulic fracture geometry, but this aspect has not been considered in this modelling work, which assumes homogeneous geomechanical properties away from well PH-1.

Validating the fracture lengths modelled during this work is a challenging task as a horizontal drilling and hydraulic fracturing campaign were not conducted at well PH-1. However, some previous hydraulic fracturing modelling has been conducted at well PH-1; notably, Gilbert (2012)'s study which also used GOHFER software to pressure match a single stage from the vertical multi-stage test. Their modelled fracture extends about 1220 m from the well, with most of the proppant emplaced within the 760 m of the well which is comparable with the result presented herein.

The differences in fracture lengths between models here-in (>500 m), Gilbert (2012)'s model (>1000 m), and the microseismic event distribution at wells PNR-1Z and PNR-2 (<350 m) is evidence of the degree of uncertainty regarding hydraulic fracture simulations. Short hydraulic fractures measured in the field may be a consequence of weaker and/or low stress intervals within the overburden (such as naturally fractured or under-pressured intervals) that favour vertical hydraulic fracture propagation over lateral propagation. But short fractures could also be explained by the presence of geomechanically weak zones near the well, such as naturally fractured intervals or faults, that dissipate the injected energy.

The long, simulated hydraulic fractures observed herein may be a consequence of the vertical heterogeneity in geomechanical properties used in the model; serving to restrict vertical fracture growth and instead, forcing hydraulic fractures over large distances within zones of uniform geomechanical properties. Furthermore, the upscaling and gridding process undertaken before simulations may also accentuate this by adding artificial boundaries between adjacent grid blocks. Fundamentally, while many very important insights can be drawn from such simulations, the precise numbers derived from these should be treated with caution.

6.2. Limitations in accounting for natural fractures

The simulations presented in this paper consider the propagation of a hydraulic, planar fracture within an intact medium. Each input grid cell contains parameters related to the strength of the rock (mainly geomechanical and stress properties) which are used in the simulation; however, the influence of a pre-existing natural fracture network on simulated hydraulic fractures are not considered. Moreover, some authors have documented the presence of natural fractures in the Bowland Shale for core and micro-imagery log data (Clarke et al., 2018; Fauchille et al., 2017).

Failure to account for natural fractures is acknowledged as a key limitation in this work. Natural fractures have been proven to have direct implications on hydraulic fracture development. As pre-existing planes of weakness, these will readily absorb energy associated with a hydraulic fracturing job, resulting in the shale matrix remaining un-fractured. Field experiments, including mine-back and core-through studies (Gale et al., 2018; Jeffrey et al., 2009; Jeffrey and Weber, 1994; Raterman et al., 2017; Warpinski et al., 1993b; Warpinski and Teufel, 1987) demonstrated that natural fractures cause branching and offset of hydraulic fractures and Weng (2015) summarised the complex ways in which a hydraulic fracture can interact with a natural fracture. Representing such a suite of interactions in a model can be challenging and many studies have presented models to address this (Dershowitz et al., 2010; Fu et al., 2011; McClure, 2012; Meyer and Bazan, 2011; Nagel et al., 2011; Savitski et al., 2013; Weng et al., 2011; Wu and Olson, 2013; Xu et al., 2009), many of which rely on simplifying assumptions that limit their applicability to specific conditions (Weng, 2015).

6.3. Implications for production potential

Assessment of the production potential of the Bowland Shale, across the UK, is still at an early stage. Probabilistic modelling of well rates conducted by NCS Reservoir Strategies (formerly Anderson Thompson Reservoir Strategies) suggests that a single, 2.5 km long well in the Bowland Shale could deliver 6.5 billion cubic feet (Bcf) of gas over 30 years, with initial 30-day production rates of about 15 million standard cubic feet per day (MMscf/day) (Edison Investment Research, 2018), though the approach to building such a model is un-published. The first production results for the shale were reported by Cuadrilla Resources following the hydraulic stimulation and partial gas flow testing of two and six stages of wells PNR-1Z and PNR-2, respectively. While only two stages were tested at well PNR-1Z, stable flow rates of 0.1 MMscf/day were reported (Cuadrilla Resources, 2019a). At well PNR-2, six stages were gas flow test, and rates between 0.06 and 0.1 MMscf/day were reported (Cuadrilla Resources, 2019b). Upscaling of these results to a 2.5 km long well would provide potential initial flow rates between 3 and 8 MMscf/day (Cuadrilla Resources, 2019b); approximately half that originally considered in the NCS Reservoir Strategies study.

Determining the potential gas resource of a shale play requires analysis of production data from numerous wells for a considerable period and forecasting using well-established methods (Bello and Wattenbarger, 2010; Cipolla et al., 2009; Terminiello et al., 2020). With the limited data available currently it is difficult to model the resource for the Bowland Shale in this manner, but an approximate insight can be ascertained from drawing on typical well production from the Marcellus Shale; an appropriate analogue play for the Bowland Shale (Harrison et al., 2019). Assuming that 13 wells (Fig. 17) with an average length of 1500 m can be drilled within this study area and taking an average gas resource of 5 Bcf for that well length (Harrison et al., 2019), the area may have the potential to produce around 65 Bcf of gas.

6.4. Stacked well potential

The modelling results presented herein suggest that there are at least two intervals in the UBS which are sufficiently stressed and thick to impede fracture height growth from overlying or underlying units. The two intervals tested lie between Landings 1 and 2 and Landings 2 and 3, which suggests that these target zones could be drilled and produced from at the same site, using stacked multilateral wells. As this work has only considered the rock properties at well PH-1, this model assumed homogeneous geology in the horizontal plane.

If production from three stacked horizontal wells can be achieved, the 65 Bcf quoted above can be multiplied by three to 195 Bcf. However, this simplistic case may not be true for actual production. The complex relationship between rock properties, hydraulic fracture propagation and fluid flow means that vertical interference is common in stacked reservoirs, even when apparent barriers exist (Shin and Popovich, 2017). The impact of production wells drilled in proximity to each other is exemplified by the growing problem of parent-child well interactions, now a common problem in mature US unconventional plays such as the Permian Basin. As operators are increasingly drilling infill (child) wells near pre-existing (parent) wells to maximise recovery, drastic variations in production are being observed. Reservoir depletion, hydraulic fracture communication (sometimes also referred to as “fracture hit”), and reservoir heterogeneity can all drive to reduce the productivity of child wells (Lindsay et al., 2018) and these limitations could apply to stacked horizontal wells too. While this specific problem may not be true if all three stacked UBS intervals are brought online at the same time it serves as a reminder of the further work that is needed to characterise the precise production strategy moving forward.

7. Conclusions

This work used hydraulic fracture modelling to design a well placement strategy for the Bowland Shale, in the region near well PH-1. The formation is situated in a geological basin that is highly faulted and folded, which causes problems relating to well placement, targeting a compartmentalised gas resource and avoiding induced seismic events. In Part 1 of this series (de Jonge-Anderson et al., 2021b), a series of geomechanical models were presented at well PH-1 and these were used to propose three landing zones within the Bowland Shale for stacked production. Stacked production might be a feasible production strategy due to the thickness of the formation, and might be crucial to ensuring the shale is commercially viable if the structural setting dictates the need for shorter horizontal wells to be drilled.

The results of hydraulic fracture simulations suggest that stacked well production is possible within the Bowland Shale and that high effective stress barriers may serve to limit vertical fracture growth and associated well interference. Simulations targeting different geomechanical intervals within well PH-1 suggest that potential fracture barriers are efficient in containing hydraulic fractures: a key concept in the stacked well production strategy. Zones of better geomechanical properties (low effective stress, low fracture toughness and high brittleness index) produced narrow and long fractures under simulation that propagate over large distances and subtle vertical changes in effective stress, since the shale’s heterogeneity appeared to limit fracture development vertically.

When horizontal pseudo-wells targeting pre-defined landing zones and a tilted, 3D geomechanical model were used, modelled hydraulic fractures propagated over large lateral distances (about 1 km), with most of the proppant placed within 500–700 m of the well. This does limit where wells could be emplaced with respect to

major, mapped faults in the area. Up to 13 well locations were identified (within a 100 km^2 area covered by 3D seismic) where laterals with length greater than 500 m could be emplaced without the modelled hydraulic fractures, or the horizontal well itself, intersecting mapped faults. Using production data from the Marcellus Shale (considered as a reasonable analogue for the Bowland Shale), it was estimated that up to 195 Bcf of gas could be produced from the area for this configuration of well placement by stacked production.

Declaration of competing interest

The authors declare that they have no known competing financial interests or personal relationships that could have appeared to influence the work reported in this paper.

Acknowledgements

Iain de Jonge-Anderson acknowledges the support of a James Watt Scholarship from Heriot-Watt University (HWU) and the receipt of a British University Funding Initiative (BUFI) studentship award (grant number GA/16S/024) from the British Geological Survey (BGS), which provides the funding for the PhD project upon which this work is based. The PhD forms part of the Natural Environment Research Council (NERC) Centre for Doctoral Training (CDT) in Oil and Gas (grant number NE/M00578X/1). The BGS is thanked for providing access to well data, Schlumberger are thanked for the provision of Techlog software and Halliburton are thanked for the provision of GOHFER software under academic license to HWU. Jingsheng Ma acknowledges NERC grant number NE/R018022/1 for financial support.

References

Andrews, I.J., 2013. The Carboniferous Bowland Shale Gas Study: Geology and Resource Estimation. British Geological Survey for the Department of Energy and Climate Change (DECC).

Barree, R.D., 1983a. A Practical Numerical Simulator for Three-Dimensional Fracture Propagation in Heterogeneous Media. SPE Reservoir Simulation Symposium. Society of Petroleum Engineers. https://doi.org/10.2118/12273-MS.

Barree, R.D., 1983b. Development of a Numerical Simulator for Three-Dimensional Hydraulic Fracture Propagation in Heterogeneous Media (PhD Thesis). Colorado School of Mines, Golden, Colorado.

Barree, R.D., 2015. Stress Shadowing and Fracture Interference in GOHFER®.

Bello, R.O., Wattenbarger, R.A., 2010. Modelling and analysis of shale gas production with a skin effect. J. Can. Petrol. Technol. 49, 37–48. https://doi.org/10.2118/143229-PA.

Belyadi, H., Fathi, E., Belyadi, F., 2017. Chapter nine - fracture pressure analysis and perforation design. In: Belyadi, H., Fathi, E., Belyadi, F. (Eds.), Hydraulic Fracturing in Unconventional Reservoirs. Gulf Professional Publishing, Boston, pp. 121–141. https://doi.org/10.1016/B978-0-12-849871-2.00009-5.

Boussinesq, J., 1885. Application des Potentiels à l'Étude de l'Équilibre et du Mouvement des Solides Élastiques, Principalement au Calcul des Déformations et des Pressions que Produisent, dans ces Solides, des Efforts Quelconques Exercés sur une Petite Partie de leur Surface ou de leur Intérieur : Mémoire suivi de Notes Étendues sur Divers Points de Physique Mathématique et D'analyse. Impr. L. Danel (Lille).

Bowker, K.A., 2003. Recent development of the Barnett shale play, fort worth basin. W. Tex. Geol. Soc. Bull. 42, 4–11.

Ciezobka, J., Courtier, J., Wicker, J., 2018. Hydraulic Fracturing Test Site (HFTS) - Project Overview and Summary of Results. https://doi.org/10.15530/URTEC-2018-2937168. SPE/AAPG/SEG Unconventional Resources Technology Conference, OnePetro.

Cipolla, C.L., Lolon, E., Mayerhofer, M.J., 2009. Reservoir Modeling and Production Evaluation in Shale-Gas Reservoirs. International Petroleum Technology Conference. https://doi.org/10.2523/IPTC-13185-MS. OnePetro.

Clarke, H., Bustin, M., Turner, P., 2014a. Unlocking the resource potential of the Bowland basin, NW England. In: SPE-167776-MS. SPE/EAGE European Unconventional Resources Conference and Exhibition. Society of Petroleum Engineers, SPE, p. 11. https://doi.org/10.2118/167776-MS.

Clarke, H., Eisner, L., Styles, P., Turner, P., 2014b. Felt seismicity associated with shale gas hydraulic fracturing: the first documented example in Europe: hydraulic fracturing, induced seismicity. Geophys. Res. Lett. 41, 8308–8314. https://doi.org/10.1002/2014GL062047.

Clarke, H., Turner, P., Bustin, R.M., Riley, N., Besly, B., 2018. Shale gas resources of the Bowland Basin, NW England: a holistic study. Petrol. Geosci. 24 (3), 287–322. https://doi.org/10.1144/petgeo2017-066.

Clarke, H., Soroush, H., Wood, T., 2019a. Preston New Road: the role of geomechanics in successful drilling of the UK's first horizontal shale gas well. In: SPE Europec Featured at 81st EAGE Conference and Exhibition. Presented at the SPE Europec Featured at 81st EAGE Conference and Exhibition. Society of Petroleum Engineers, London, England, UK. https://doi.org/10.2118/195563-MS.

Clarke, H., Verdon, J.P., Kettlety, T., Baird, A.F., Kendall, J.M., 2019b. Real time imaging, forecasting, and management of human-induced seismicity at Preston New Road, Lancashire, England. Seismol Res. Lett. 90 (5), 1902–1915. https://doi.org/10.1785/0220190110.

Cuadrilla Resources, 2019a. Cuadrilla shale gas initial flow test results. URL. https://cuadrillaresources.uk/cuadrilla-shale-gas-initial-flow-test-results/. accessed 8.17.20.

Cuadrilla Resources, 2019b. Update on flow testing of second shale well at preston New Road. URL. https://cuadrillaresources.uk/update-on-flow-testing-of-second-shale-well-at-preston-new-road/. accessed 8.17.20.

de Jonge-Anderson, I., Underhill, J.R., 2020. Structural constraints on lower carboniferous shale gas exploration in the Craven Basin, NW England. Petrol. Geosci. 26, 303–324. https://doi.org/10.1144/petgeo2019-125.

de Jonge-Anderson, I., Ma, J., Wu, X., Stow, D., 2021a. Determining reservoir intervals in the Bowland Shale using petrophysics and rock physics models. Geophys. J. Int. 228, 39–65. https://doi.org/10.1093/gji/ggab334.

de Jonge-Anderson, I., Ma, J., Wu, X., Stow, D., Griffiths, D., 2021b. Bowland Shale well placement strategy – Part 1: determining landing intervals using geomechanical properties. Mar. Petrol. Geol. 133, 105277. https://doi.org/10.1016/j.marpetgeo.2021.105277.

De Pater, H., Pellicer, M., 2011. Geomechanical Study of Bowland Shale Seismicity – Fracture Geometry and Injection Mechanism. StrataGen Delft BV, Delft, the Netherlands.

Dershowitz, W.S., Cottrell, M.G., Lim, D.H., Doe, T.W., 2010. A Discrete Fracture Network Approach for Evaluation of Hydraulic Fracture Stimulation of Naturally Fractured Reservoirs. The 44th U.S. Rock Mechanics Symposium and 5th U.S.-Canada Rock Mechanics Symposium. American Rock Mechanics Association.

Edison Investment Research, 2018. AJ Lucas Group - Dominant Bowland shale position [WWW Document]. Edison. URL. https://www.edisongroup.com/publication/dominant-bowland-shale-position/20787/. accessed 8.17.20.

Emmings, J.F., Davies, S.J., Vane, C.H., Moss-Hayes, V., Stephenson, M.H., 2020. From marine bands to hybrid flows: sedimentology of a Mississippian black shale. Sedimentology 67, 261–304. https://doi.org/10.1111/sed.12642.

Fauchille, A.L., Ma, L., Rutter, E., Chandler, M., Lee, P.D., Taylor, K.G., 2017. An enhanced understanding of the Basinal Bowland shale in Lancashire (UK), through microtextural and mineralogical observations. Mar. Petrol. Geol. 86, 1374–1390. https://doi.org/10.1016/j.marpetgeo.2017.07.030.

Fisher, M.K., Heinze, J.R., Harris, C.D., Davidson, B.M., Wright, C.A., Dunn, K.P., 2004. Optimizing Horizontal Completion Techniques in the Barnett Shale Using Microseismic Fracture Mapping. The SPE Annual Technical Conference and Exhibition. Society of Petroleum Engineers. https://doi.org/10.2118/90051-MS.

Fu, P., Johnson, S.M., Carrigan, C.R., 2011. Simulating Complex Fracture Systems in Geothermal Reservoirs Using an Explicitly Coupled Hydro-Geomechanical Model. The 45th U.S. Rock Mechanics/Geomechanics Symposium. American Rock Mechanics Association.

Gale, J.F.W., Elliott, S.J., Laubach, S.E., 2018. Hydraulic Fractures in Core from Stimulated Reservoirs: Core Fracture Description of HFTS Slant Core. West Texas. Midland Basin, OnePetro. https://doi.org/10.15530/URTEC-2018-2902624. The SPE/AAPG/SEG Unconventional Resources Technology Conference.

Gilbert, J., 2012. Cuadrilla Resources Preese Hall #1 Stage 2 Fracture Height Growth.

Halliburton, 2019. GOHFER 3D User Manual.

Harrison, B., Oueidat, T., Falcone, G., 2019. Selecting an Appropriate Unconventional Play Analog for the Bowland Shale while Acknowledging Operational Constraints in the UK. The 2019 AAPG Annual Convention & Exhibition. AAPG Search and Discovery, San Antonio, Texas, USA, p. 21. https://doi.org/10.1306/11252Harrison2019.

Jeffrey, R.G., Bunger, A., 2009. A detailed comparison of experimental and numerical data on hydraulic fracture height growth through stress contrasts. SPE J. 14 (3), 413–422. https://doi.org/10.2118/106030-PA.

Jeffrey, R.G., Weber, C.R., 1994. Hydraulic Fracturing Experiments in the Great Northern Coal Seam. The SPE Asia Pacific Oil and Gas Conference. Society of Petroleum Engineers. https://doi.org/10.2118/28779-MS.

Jeffrey, R.G., Bunger, A., LeCampion, B., Zhang, X., Chen, Z., van As, A., Allison, D.P., De Beer, W., Dudley, J.W., Siebrits, E., Thiercelin, M.J., Mainguy, M., 2009. Measuring Hydraulic Fracture Growth in Naturally Fractured Rock. The SPE Annual Technical Conference and Exhibition. Society of Petroleum Engineers. https://doi.org/10.2118/124919-MS.

Lindsay, G., Miller, G., Xu, T., Shan, D., Baihly, J., 2018. Production Performance of Infill Horizontal Wells vs. Pre-existing Wells in the Major US Unconventional Basins. The SPE Hydraulic Fracturing Technology Conference and Exhibition. Society of Petroleum Engineers. https://doi.org/10.2118/189875-MS.

Mack, M.G., Warpinski, N., 2000. Mechanics of hydraulic fracturing. In: Reservoir Stimulation. Wiley-Blackwell.

McClure, M.W., 2012. Modeling and Characterization of Hydraulic Stimulation and Induced Seismicity in Geothermal and Shale Gas Reservoirs (PhD Thesis). Stanford University.

McKenna, J.P., 2014. Where Did the Proppant Go? the SPE/AAPG/SEG

Unconventional Resources Technology Conference. Unconventional Resources Technology Conference. https://doi.org/10.15530/URTEC-2014-1922843.
Meyer, B.R., Bazan, L.W., 2011. A Discrete Fracture Network Model for Hydraulically Induced Fractures - Theory, Parametric and Case Studies. The SPE Hydraulic Fracturing Technology Conference. Society of Petroleum Engineers. https://doi.org/10.2118/140514-MS.
Morrill, J.C., Miskimins, J.L., 2012. Optimizing Hydraulic Fracture Spacing in Unconventional Shales. The SPE Hydraulic Fracturing Technology Conference. https://doi.org/10.2118/152595-MS. OnePetro.
Mullen, J., 2010. Petrophysical Characterization of the Eagle Ford Shale in South Texas. The Canadian Unconventional Resources and International Petroleum Conference. Society of Petroleum Engineers. https://doi.org/10.2118/138145-MS.
Nagel, N.B., Sanchez-Nagel, M., 2011. Stress Shadowing and Microseismic Events: A Numerical Evaluation. The SPE Annual Technical Conference and Exhibition. Society of Petroleum Engineers. https://doi.org/10.2118/147363-MS.
Nagel, N.B., Gil, I., Sanchez-Nagel, M.A., Damjanac, B., 2011. Simulating hydraulic fracturing in real fractured rocks - Overcoming the limits of pseudo-3D models. The SPE Hydraulic Fracturing Technology Conference. Society of Petroleum Engineers.
Nagel, N.B., Zhang, F., Sanchez-Nagel, M.A., Lee, B., Agharazi, A., 2013a. Stress Shadow Evaluations for Completion Design in Unconventional Plays. The SPE Unconventional Resources Conference Canada. Society of Petroleum Engineers. https://doi.org/10.2118/167128-MS.
Nagel, N.B., Sanchez-Nagel, M.A., Zhang, F., Garcia, X., Lee, B., 2013b. Coupled numerical evaluations of the geomechanical interactions between a hydraulic fracture stimulation and a natural fracture system in shale formations. Rock Mech. Rock Eng. 46, 581–609. https://doi.org/10.1007/s00603-013-0391-x.
North Sea Transition Authority, 2019. Preston New Road - PNR 1Z - hydraulic fracturing operations data [WWW Document]. URL. https://www.nstauthority.co.uk/exploration-production/onshore/onshore-reports-and-data/preston-new-road-pnr-1z-hydraulic-fracturing-operations-data/. accessed 8.19.20.
Parsegov, S.G., Nandlal, K., Schechter, D.S., Weijermars, R., 2018. Physics-driven Optimization of Drained Rock Volume for Multistage Fracturing: Field Example from the Wolfcamp Formation, Midland Basin. The SPE/AAPG/SEG Unconventional Resources Technology Conference, Unconventional Resources Technology Conference. https://doi.org/10.15530/URTEC-2018-2879159.
Pollastro, R.M., Jarvie, D.M., Hill, R.J., Adams, C.W., 2007. Geologic framework of the mississippian Barnett shale, barnett-paleozoic total petroleum system, bend arch-fort worth basin, Texas. AAPG (Am. Assoc. Pet. Geol.) Bull. 91 (4), 405–436. https://doi.org/10.1306/10300606008.
Ramurthy, M., Hendrickson, R.B., 2007. Effects of High Pressure Dependent Leakoff and High Process Zone Stress in Coal Stimulation Treatments. The Rocky Mountain Oil & Gas Technology Symposium. Society of Petroleum Engineers. https://doi.org/10.2118/107971-MS.
Raterman, K.T., Farrell, H.E., Mora, O.S., Janssen, A.L., Gomez, G.A., Busetti, S., McEwen, J., Davidson, M., Friehauf, K., Rutherford, J., Reid, R., Jin, G., Roy, B., Warren, M., 2017. Sampling a Stimulated Rock Volume: an Eagle Ford Example. The SPE/AAPG/SEG Unconventional Resources Technology Conference. https://doi.org/10.15530/URTEC-2017-2670034. OnePetro.
Raterman, K.T., Farrell, H.E., Mora, O.S., Janssen, A.L., Gomez, G.A., Busetti, S., McEwen, J., Friehauf, K., Rutherford, J., Reid, R., Jin, G., Roy, B., Warren, M., 2018. Sampling a stimulated rock volume: an Eagle Ford example. SPE Reservoir Eval. Eng. 21, 927–941. https://doi.org/10.2118/191375-PA.
Raterman, K., Liu, Y., Warren, L., 2019. Analysis of a Drained Rock Volume: an Eagle Ford Example. The SPE/AAPG/SEG Unconventional Resources Technology Conference, OnePetro. https://doi.org/10.15530/urtec-2019-263.
Rios, A.M., Gutiérrez, G., Nagel, N.B., Zhang, F., Sanchez-Nagel, M.A., Lee, B., 2013. Stress Shadow Evaluations for Chicontepec – Evaluating New Completion Options. The 47th U.S. Rock Mechanics/Geomechanics Symposium. American Rock Mechanics Association.
Rutledge, J., Leaney, S., Best, J., Craven, M., Swafford, L., 2018. High-resolution Microseismic-Source Locations and Moment-Tensor Solutions from the Permian Basin. The 2018 SEG International Exposition and Annual Meeting. Society of Exploration Geophysicists.
Savitski, A.A., Lin, M., Riahi, A., Damjanac, B., Nagel, N.B., 2013. Explicit Modeling of Hydraulic Fracture Propagation in Fractured Shales. The International Petroleum Technology Conference, International Petroleum Technology Conference. https://doi.org/10.2523/IPTC-17073-MS.
Shin, D., Popovich, D., 2017. Optimizing Vertical and Lateral Spacing of Horizontal Wells in Permian Basin Stacked Bench Developments. The SPE/AAPG/SEG Unconventional Resources Technology Conference, Unconventional Resources Technology Conference. https://doi.org/10.15530/URTEC-2017-2669025.
Simonson, E.R., Abou-Sayed, A.S., Clifton, R.J., 1978. Containment of massive hydraulic fractures. Soc. Petrol. Eng. J. 18 (1), 27–32. https://doi.org/10.2118/6089-PA.
Simpson, M.D., Patterson, R., Wu, K., 2016. Study of Stress Shadow Effects in Eagle Ford Shale: Insight from Field Data Analysis. The 50th U.S. Rock Mechanics/Geomechanics Symposium. American Rock Mechanics Association.
Skomorowski, N., Dussealut, M.B., Gracie, R., 2015. The Use of Multistage Hydraulic Fracture Data to Identify Stress Shadow Effects. The 49th U.S. Rock Mechanics/Geomechanics Symposium. American Rock Mechanics Association.
Smith, N., Turner, P., Williams, G., 2010. UK data and analysis for shale gas prospectivity. In: Petroleum Geology: from Mature Basins to New Frontiers—Proceedings of the 7th Petroleum Geology Conference. Geological Society of London, pp. 1087–1098. https://doi.org/10.1144/0071087.
Stegent, N., Candler, C., 2018. Downhole Microseismic Mapping of More than 400 Fracturing Stages on a Multiwell Pad at the Hydraulic Fracturing Test Site (HFTS): Discussion of Operational Challenges and Analytic Results. The SPE/AAPG/SEG Unconventional Resources Technology Conference, Unconventional Resources Technology Conference. https://doi.org/10.15530/URTEC-2018-2902311.
Terminiello, A., Crespo, P., Nasca, M., 2020. Evaluating the Performance of Decline Curve Analysis Equations during the Early Life of a Well through the Quantification of the Uncertainty Associated with the Estimated Ultimate Recovery in a Shale Oil and Gas Formation. Presented at the SPE/AAPG/SEG Latin America Unconventional Resources Technology Conference. https://doi.org/10.15530/urtec-2020-1518. OnePetro.
Verdon, J.P., Kettlety, T., Kendall, J.-M., 2019. Geomechanical Interpretation of Microseismicity at the Preston New Road PNR-1z Well, Lancashire, England. Oil and Gas Authority, London.
Verdon, J.P., Kettlety, T., Kendall, J.-M., 2020. Geomechanical Interpretation of Induced Seismicity at the Preston New Road PNR-2 Well, Lancashire, England. Oil and Gas Authority, London.
Warpinski, N.R., Teufel, L.W., 1987. Influence of geologic discontinuities on hydraulic fracture propagation (includes associated papers 17011 and 17074). J. Petrol. Technol. 39, 209–220. https://doi.org/10.2118/13224-PA.
Warpinski, N.R., Abou-Sayed, I.S., Moschovidis, Z., Parker, C., 1993a. Hydraulic Fracture Model Comparison Study: Complete Results (No. SAND-93-7042; GRI-93/0109). Sandia National Labs, Albuquerque, NM. https://doi.org/10.2172/10176839. United States); Gas Research Inst., Chicago, IL (United States).
Warpinski, N.R., Lorenz, J.C., Branagan, P.T., Myal, F.R., Gall, B.L., 1993b. Examination of a cored hydraulic fracture in a deep gas well (includes associated papers 26302 and 26946). SPE Prod. Facil. 8, 150–158. https://doi.org/10.2118/22876-PA.
Weng, X., 2015. Modeling of complex hydraulic fractures in naturally fractured formation. J. Unconv. Oil Gas Resour. 9, 114–135. https://doi.org/10.1016/j.juogr.2014.07.001.
Weng, X., Kresse, O., Cohen, C.-E., Wu, R., Gu, H., 2011. Modeling of hydraulic-fracture-network propagation in a naturally fractured formation. SPE Prod. Oper. 26, 368–380. https://doi.org/10.2118/140253-PA.
Whitelaw, P., Uguna, C.N., Stevens, L.A., Meredith, W., Snape, C.E., Vane, C.H., Moss-Hayes, V., Carr, A.D., 2019. Shale gas reserve evaluation by laboratory pyrolysis and gas holding capacity consistent with field data. Nat. Commun. 10, 3659. https://doi.org/10.1038/s41467-019-11653-4.
Wu, K., Olson, J.E., 2013. Investigation of Critical in Aitu and Injection Factors in Multi-Frac Treatments: Guidelines for Controlling Fracture Complexity. The SPE Hydraulic Fracturing Technology Conference. Society of Petroleum Engineers. https://doi.org/10.2118/163821-MS.
Xu, W., Le Calvez, J.H., Thiercelin, M.J., 2009. Characterization of Hydraulically-Induced Fracture Network Using Treatment and Microseismic Data in a Tight-Gas Sand Formation: A Geomechanical Approach. Society of Petroleum Engineers. https://doi.org/10.2118/125237-MS. The SPE Tight Gas Completions Conference.
Xu, W., Prioul, R., Berard, T., Weng, X., Kresse, O., 2019. Barriers to Hydraulic Fracture Height Growth: A New Model for Sliding Interfaces. The SPE Hydraulic Fracturing Technology Conference and Exhibition. https://doi.org/10.2118/194327-MS. OnePetro.
Zhang, J.J., 2019. Chapter 11 - geomechanics applications in hydraulic fracturing. In: Zhang, J.J. (Ed.), Applied Petroleum Geomechanics. Gulf Professional Publishing, pp. 441–481. https://doi.org/10.1016/B978-0-12-814814-3.00011-3.